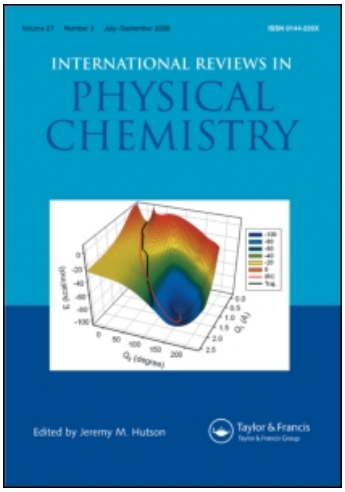


**International Reviews in Physical Chemistry**
Publication details, including instructions for authors and subscription information:
http://www.informaworld.com/smpp/title~content=t713724383

# Experimental Versus Theoretical Electron Densities. Small Molecules, Large Molecules, and Salts

Martin Breitenstein[ab]; Helmut Dannöhl[ab]; Hermann Meyer[ab]; Armin Schweig[ab]; Rolf Seeger[ab]; Ute Seeger[ab]; Werner Zittlal[ab]
[a] Fachbereich Physikalische Chemie, Universitdt Marburg, Marburg, Federal Republic of Germany [b] Fachbereich Chemie, Universität Kaiserslautern, Kaiserslautern, Federal Republic of Germany

**To cite this Article** Breitenstein, Martin , Dannöhl, Helmut , Meyer, Hermann , Schweig, Armin , Seeger, Rolf , Seeger, Ute and Zittlal, Werner(1983) 'Experimental Versus Theoretical Electron Densities. Small Molecules, Large Molecules, and Salts', International Reviews in Physical Chemistry, 3: 3, 335 — 391
**To link to this Article: DOI:** 10.1080/01442358309353349
**URL:** http://dx.doi.org/10.1080/01442358309353349

*International Reviews in Physical Chemistry* (1983), *3* (335–391)

# EXPERIMENTAL VERSUS THEORETICAL ELECTRON DENSITIES. SMALL MOLECULES, LARGE MOLECULES, AND SALTS[1,2]

MARTIN BREITENSTEIN[3a], HELMUT DANNÖHL[3a], HERMANN MEYER[3a], ARMIN SCHWEIG[3a], ROLF SEEGER[3b], UTE SEEGER[3b] AND WERNER ZITTLAU[3a]

*Fachbereich Physikalische Chemie, Universität Marburg, D-3550 Marburg, Federal Republic of Germany, and the Fachbereich Chemie, Universität Kaiserslautern, D-6750 Kaiserslautern, Federal Republic of Germany*



## ABSTRACT

High quality *ab initio* calculations of electron deformation densities and comparisons with available experimental results are presented for small molecules. AHF (approximate Hartree–Fock) basis set and electron correlation effects are assessed. The high quality of the 4–31G + BF (bond functions) basis set for the computation of deformation densities is established for small molecules. Comparison of 4–31G + BF electron densities with all available experimental data is made for some selected large organic molecules. Errors and problems in the experimental and theoretical methods are discussed. Crystal effects such as hydrogen bonding and ion effects in salts are estimated. It is shown that all the effects considered (i.e., near HF basis set, correlation, hydrogen bonding and ion effects) are small compared to possible experimental uncertainties. Thus, at present, economical 4–31G + BF calculations of isolated molecules are sufficiently accurate for comparisons with any type of experimental determination in gas or solid phases.

## 1. INTRODUCTION

Electron densities play an important role in every chemist's thinking. Therefore, much work has been devoted to the measurement and calculation of this function[4–20].

When we started our work in 1975 few comparisons between calculated and measured densities were available. This was mainly because the electron density was measured in a crystal, where the individual molecules are undergoing internal and lattice vibrations, whereas the quantum-chemical calculation is usually made for an isolated molecule at rest. The resulting so-called static density has to be vibrationally averaged (or thermally smeared) to get the so-called dynamic density before a meaningful comparison between the theoretical and experimental densities can be made. This problem was overcome by developing a simple generally applicable approximate vibrational averaging procedure[21].

Mainly for crystallographic reasons, most experimental electron density distributions have been determined for crystals built up from rather large molecules. Whereas for small molecules large STO (Slater-type orbital) or GTO (Gaussian-type

0144-235X/83/03 0335-57 $03.00 

orbital) basis sets can be used in AHF (approximate Hartree–Fock) calculations of electron densities, this becomes increasingly prohibitive for larger molecules, for computational reasons. It was therefore an important goal to find an economical basis set that mimics NHF (near Hartree–Fock) electron density distributions. Such a basis set, 4–31G + BF (bond functions), was previously[22] proposed. Below, it will be considered in much more detail.

In recent years, crystallographers turned more to crystals made from smaller molecules, with the object of testing quantum-chemical methods. In addition, charge density distributions of the diatomics $N_2$ and $O_2$ were derived from electron diffraction measurements in the gaseous phase. Discrepancies between calculated and experimental densities that were detected in these cases were often attributed *ad hoc* to the neglect of electron correlation in the electron density calculations. This uncertainty induced us to develop the PERTCI (a configurational interaction) method[23] and to undertake large scale CI calculations of electron density distributions[24]. A full account of these results is given below.

Electron densities that are based on X-ray diffraction for crystals are 'molecular' densities in a crystal, i.e., subject to effects of intermolecular forces. Commonly, calculated densities refer to an isolated molecule. Since discrepancies between calculated and measured densities are often referred *ad hoc* to the neglect of crystal effects in the calculations, we carried out some model calculations for hydrogen-bonded systems and ion crystals (sodium salts[25]). It is surprising that, even in these cases of strong interactions, effects in electron densities are only minor. A detailed comparison between theory and experiment is presented below.

A major problem in experimental electron density determinations is that there may still be appreciable systematic errors whose magnitude is not known with certainty and can vary from case to case[26,27]. On the other hand, quantum-chemical results are also subject to model (systematic) errors of which the most important are the basis set and correlation errors. Since, however, these errors can be estimated on the base of high-quality calculations (HF and NHF CI) for some small molecules[27] and the 4–31G + BF basis set error can be determined with respect to NHF densities, some assessment of the accuracy of experimental electron densities is possible. Thus for small molecules it was concluded that, at present, experimental electron density determinations have no chance to outperform corresponding theoretical calculations[27]. For larger molecules both approaches are at approximately equal levels. The full material for these important conclusions is presented below.

In order to achieve our various goals in a logical way, we present the calculational material in the following sequence:

1. High-quality calculations for small molecules and comparison of available experimental material with the calculated results; assessment of correlation effects.
2. Comparison of 4–31G + BF results with NHF results; assessment of the 4–31G + BF basis set error relative to NHF results.
3. Comparison of 4–31G + BF electron densities with all available corresponding experimental material for some selected large organic molecules; discussion of problems and errors.
4. Estimation of strong crystal effects such as hydrogen bonding and ion effects on electron densities for some selected examples.

## 2. THEORETICAL APPROACH AND DEFINITION OF DEFORMATION DENSITIES

The one-electron probability density distribution or simply the electron density $\varrho(\vec{r})$, where $\vec{r}$ is a point in space, is usually discussed in electron density work in terms of the deformation density[28] (or electron density difference[29], Roux function, or bond density[30])

$$\Delta\varrho(\vec{r}) = \varrho(\vec{r}) - \varrho(\vec{r})_{\mathrm{IAM}} \tag{1}$$

$\varrho(\vec{r})_{\mathrm{IAM}}$ is the density distribution of the independent-atom model (or free-, or isolated-atom model). In this model, the density is the superposition of the densities of the constituent atoms centered at the nuclear positions of the system. Commonly, spherically averaged densities of the individual atoms are used.

Since the X-ray diffraction workers generally use $\varrho(\vec{r})_{\mathrm{IAM}}$ built up from (relativistic) HF (Hartree–Fock) atomic densities, all theoretical deformation densities of the present work are referred to the AHF IAM density $\varrho_{\mathrm{AHF}}(\vec{r})_{\mathrm{IAM}}$. The atomic densities are calculated with the Roothaan open-shell procedure[31] using the same AHF basis sets as for the corresponding molecular calculations[32]. Molecular densities $\varrho(\vec{r})$ are considered both in the AHF and AHF CI approach and designated as $\varrho_{\mathrm{AHF}}(\vec{r})$ and $\varrho_{\mathrm{AHF\ CI}}(\vec{r})$, respectively. Accordingly, we distinguish between the AHF and AHF CI (correlated) deformation densities of Eqs. (2) and (3):

$$\Delta\varrho_{\mathrm{AHF}}(\vec{r}) = \varrho_{\mathrm{AHF}}(\vec{r}) - \varrho_{\mathrm{AHF}}(\vec{r})_{\mathrm{IAM}} \tag{2}$$

$$\Delta\varrho_{\mathrm{AHF\ CI}}(\vec{r}) = \varrho_{\mathrm{AHF\ CI}}(\vec{r}) - \varrho_{\mathrm{AHF}}(\vec{r})_{\mathrm{IAM}} \tag{3}$$

Effects of electron correlation can be directly seen from the correlation density $\Delta\varrho_{\mathrm{corr,\ AHF}}(\vec{r})$

$$\Delta\varrho_{\mathrm{corr,\ AHF}}(\vec{r}) = \varrho_{\mathrm{AHF\ CI}}(\vec{r}) - \varrho_{\mathrm{AHF}}(\vec{r}) \tag{4}$$

Throughout this work basis sets of CGTOs (contracted GTOs) are used.

The AHF calculations were carried out using the GAUSSIAN 70[33], GAUSSIAN 76[34], GAUSSIAN 76 with parts integrated from GAUSSIAN 80[35], the GAUSSIAN 80[36] and the POLYATOM[37] program systems. GAUSSIAN 70 was implemented on a Telefunken TR 440, GAUSSIAN 76 both on a Telefunken TR 440 and a CDC Cyber 174, the combined GAUSSIAN 76/80 on the TR 440, GAUSSIAN 80 on a Perkin Elmer 8/32 applying parallel processing techniques[38], and POLYATOM on both the TR 440 and IBM 370/168. Present computer and program conditions limit the maximum number of basis orbitals to be used, as follows: 70 for the GAUSSIAN 70, 90 (TR 440) and 150 (Cyber 174) for the GAUSSIAN 76, 127 for the Perkin Elmer 8/32, and 80 (TR 440) and 90 (IBM 370/168) for POLYATOM.

Correlated molecular wavefunctions were computed with the PERTCI program system. The method has been described in detail[39]. Only a few essential points will be reviewed. Suppose that the molecular ground state can be characterized by one MC (main configuration) $\psi_0$. For a reasonably complete treatment of correlation, the configuration space will include all spin and symmetry adapted configurations which are SECs (singly excited configurations) or DECs (doubly excited configurations) with respect to the main configuration. At first a SELCI (selected CI)

calculation is carried out. The SELCI space consists of the MC, all SECs and those DECs $\psi_i$ whose interaction $|H_{oi}|^2(E_i - E_o)^{-1}$ (matrix element $H_{oi}$ and AHF configuration energies $E_i$ and $E_o$) with the MC $\psi_o$ exceeds a threshold value $T$. The resulting lowest energy SELCI wavefunction is further improved by taking account of the remaining (i.e., not selected for SELCI) DECs by second-order Brillouin–Wigner perturbation theory. The resulting PERTCI wavefunction is then used to calculate $\Delta\varrho_{\mathrm{AHF\,CI}}(\vec{r})$.

The PERTCI program is implemented on a Telefunken TR 440 computer. The largest PERTCI calculation that has been carried out, in connection with the present work, deals with about 90 000 configurations.

As mentioned in the Introduction, the experimental X-ray deformation densities are dynamic densities. Therefore the static theoretical densities $\Delta\varrho_{\mathrm{AHF}}(\vec{r})$ or $\Delta\varrho_{\mathrm{AHF\,CI}}(\vec{r})$ have to be vibrationally averaged before the experimental densities can be contrasted with the theoretical ones. For computational reasons, exact vibrational averaging over the internal and lattice vibrations is not possible. Therefore, we introduced an approximate procedure that makes use of experimental data, namely the X-ray or neutron atomic vibration tensors $\boldsymbol{U}_k$ or the tensors $\boldsymbol{T}$ (translation), $\boldsymbol{L}$ (libration) and $\boldsymbol{S}$ (screw tensor that describes the coupling between translation and libration). The $\boldsymbol{T}$, $\boldsymbol{L}$, and $\boldsymbol{S}$ tensors can be determined either directly or, under favorable circumstances, from the measured $\boldsymbol{U}_k$; conversely the $\boldsymbol{U}_k$ can be calculated from experimentally available $\boldsymbol{T}$, $\boldsymbol{L}$, $\boldsymbol{S}$ tensors. The method has been described in detail[21,27]. Therefore, only a few remarks need be added. One molecule of which the static density has been calculated before is enclosed in an orthorhombic pseudo-unit cell, with lattice parameters $|\vec{a}|$, $|\vec{b}|$, and $|\vec{c}|$ chosen large enough as to make overlap of electron density from neighboring cells negligible. The X-ray structure factors are then evaluated for this pseudo-crystal making use of the convolution approximation[40]. Approximate temperature factors for the individual density units $\phi_\mu\phi_\nu$($\phi_\mu$ and $\phi_\nu$ are members of the CGTO basis set) are calculated from the $\boldsymbol{U}_k$ and/or the $\boldsymbol{T}\,\boldsymbol{L}\,\boldsymbol{S}$ tensors. Finally, an approximate dynamic deformation density is obtained by Fourier synthesis. In this synthesis, the same $\sin\theta/\lambda$ (Bragg angle $\theta$, X-ray wavelength $\lambda$) is used as in the corresponding experimental synthesis. In this way, possible effects of the finite experimental resolution are elegantly taken account of.

Vibrationally averaged deformation densities are often written as $<\Delta\varrho(\vec{r})>$. Due to the large amplitudes of lattice vibrations, bonding and lone-pair regions of $<\Delta\varrho(\vec{r})>$ are normally reduced by roughly 50% relative to $\Delta\varrho(\vec{r})$. Since all comparisons between X-ray and theoretical deformation densities are made on the basis of dynamic densities in the present paper, we omit parentheses throughout and also write $\Delta\varrho(\vec{r})$ for the dynamic densities. Note, however, that the experimental electron diffraction deformation densities currently available are static ones.

The experimental counterparts to $\Delta\varrho_{\mathrm{AHF}}(\vec{r})$ or $\Delta\varrho_{\mathrm{AHF\,CI}}(\vec{r})$ are the so-called X–N, X–X, M–A, and ED deformation densities $\Delta\varrho_{\mathrm{X-N}}(\vec{r})$, $\Delta\varrho_{\mathrm{X-X}}(\vec{r})$, $\Delta\varrho_{\mathrm{M-A}}(\vec{r})$, and $\Delta\varrho_{\mathrm{ED}}(\vec{r})$, respectively.

The X–N, X–X, and M–A deformation densities are derived from Fourier difference syntheses. Both the X–N and X–X densities are based on the measured amplitudes of X-ray structure factors and phases from conventional or model density refinements for the representation of $\varrho(\vec{r})$, with finite resolution, and on atomic form factors and either neutron (X–N) or high-order X-ray (X–X) positional and thermal parameters for the representation of $\varrho(\vec{r})_{\mathrm{IAM}}$, with finite resolution. Sometimes neutron and high-order X-ray parameters are mixed in some way or other. We refer to these densities then as X–N/X densities.

M–A densities are based on aspherical atom density models on the one hand (with the multipole density as the best known) and bond density models on the other and the structure factors (both amplitudes and phases) derived from the corresponding refinements. Variants have come into usage for the representation of the M state (i.e., $\varrho(\vec{r})$) and the A state (i.e., $\varrho(\vec{r})_{IAM}$) within the M–A densities. Instead of taking both the amplitudes and phases from the molecular (M) refinement, experimental amplitudes and phases from the refinement can be combined. Positional and thermal parameters can be taken from the M refinement or they can be fixed to neutron or high-order parameters or a mixture of both sorts. We come back to the various types of experimental X-ray deformation densities when practical examples are discussed below.

The $\Delta\varrho_{ED}(\vec{r})$ densities that have become known so far are of the M–A variety. An aspherical model density is assumed and the total intensity of scattered electrons is written as a function of the parameters of the model density. The parameters are determined by a least-squares fit of the model expression to the measured intensity distribution.

## 3. RESULTS AND DISCUSSION

### *3.1 Small molecules: deformation density standards by high-quality* ab initio *calculations*

The following molecules are considered: $N_2$, $O_2$, $F_2$, CO, $H_2O$, HC≡CH, and $H_2O_2$.

For all molecules experimental geometries have been used: $N_2$[41] R = 1.0950 Å, $O_2$[42] R = 1.207 Å, $F_2$[41] R = 1.4177 Å, CO[43] R = 1.128 Å, $H_2O$[41] R = 0.9572 Å, ∢ HOH = 104.52°, HC≡CH[43] R(CC) = 1.2028 Å, R(CH) = 1.0597 Å, and $H_2O_2$[44] R(OO) = 1.458 Å, R(OH) = 0.988 Å, ∢ HOOH = 90.2°, ∢ OOH = 101.9° (equilibrium distance R, bond or dihedral angle ∢).

The AF (atomic function) basis sets used, the AHF energies attained with these sets along with the HF or estimated HF limits, the PERTCI threshold parameter $T$, the number of SECs and DECs involved in each PERTCI calculation, as well as $E_{corr}$(correlation energy) given as a percentage of the total correlation energy, are summarized in *Table 1*. Generally all DECs are included in the PERTCI calculations except for $O_2$, where the total number of 70 096 DECs was reduced by selection to 25 354 to save computer time.

Some test calculations concerning the flexibility of the basis sets used have been performed (for $N_2$, cf. Ref. 24). In all cases the deformation densities obtained with the final sets of *Table 1* have sufficiently converged. In all cases in *Table 1*, PERTCI recovers 60–70% of the correlation energy.

Amongst the molecules considered here, exact numerical HF solutions are known for $N_2$[45], CO[45], and $F_2$[46]. Unfortunately, no maps of $\varrho_{HF}(\vec{r})$ or $\Delta\varrho_{HF}(\vec{r})$ have been published. However for $N_2$ and CO, MO (molecular orbital) densities and differences between the HF MO densities and MO densities based on the STO NHF wavefunction of Ref. 47 are available. From these results, it can be estimated that the difference function $\varrho_{HF}(\vec{r}) - \varrho_{AHF}(\vec{r})$ (AHF: present work) does not exceed 0.1 e/Å$^3$ at the midpoint of the N≡N and C≡O bonds. It can be expected[27] that the deviation in the deformation density at the midpoint of a bond will be nearly the same as in the molecular density itself.

In view of the large CGTO basis sets used, the basis set error in the deformation density appears to be rather pronounced. It is interesting to note that the NHF density of $N_2$ that is based on the wavefunction of Ref. 47 (NHF energy only about

TABLE 1. Details of the CGTO AHF and PERTCI calculations

| Molecule | AF[a] | | $-E_{HF}$ (hartree)[b] | | T[c] (eV) | SEC[d] | DEC[e] | $E_{corr}$ (%)[f] |
|---|---|---|---|---|---|---|---|---|
| $N_2$ | 78 | (11s7p2d1f)/ [5s4p2d1f][g] | AHF | 108.9866 | 0.01 | 93 | 17650 | 71[n] |
| | | s: 5,1,2,2,1 | HF limit | 108.9939[ℓ] | | | | |
| | | p: 4,1,1,1[g] | | | | | | |
| $O_2$ | 70 | (13s8p2d)/ [8s5p2d][h] | AHF | 149.6614 | 0.01 | 294 | 25354 | 69[o] |
| | | s: 5,2,1,1,1,1,1,1 | HF limit | $149.670 \pm 0.003$[m] | | | | |
| | | p: 4,1,1,1,1 | | | | | | |
| $F_2$ | 58 | (11s7p2d)/ [5s4p2d][g] | AHF | 198.7508 | 0.02 | 82 | 13498 | 62[p] |
| | | s: 5,3,1,1,1 | HF limit | $198.780 \pm 0.003$[m] | | | | |
| | | p: 4,1,1,1[g] | | | | | | |
| CO | 60 | C,O (10s6p2d)/ [6s4p2d][i] | AHF | 112.7813 | 0.01 | 157 | 20788 | 67[p] |
| | | s: 5,1,1,1,1,1 | HF limit | 112.7910[ℓ] | | | | |
| | | p: 3,1,1,1[i] | | | | | | |
| $H_2O$ | 41 | O (11s7p2d)/ [5s4p2d][g] | AHF | 76.0528 | 0.01 | 67 | 4619 | 64[p] |
| | | s: 5,2,1,2,1 | HF limit | $76.070 \pm 0.005$[m] | | | | |
| | | p: 4,1,1,1,[g] | | | | | | |
| | | H (6s1p)/[3s1p][g] | | | | | | |
| | | s: 3,2,1[g] | | | | | | |
| HC≡CH | 80 | C (10s6p2d)/ [6s4p2d][i] | AHF | 76.8487 | 0.01 | 111 | 20504 | 66[p] |
| | | s: 5,1,1,1,1,1 | HF limit | $76.858 \pm 0.002$[m] | | | | |
| | | p: 3,1,1,1[i] | | | | | | |
| | | H (6s2p)/[4s2p][j] | | | | | | |
| | | s: 3,1,1,1[j] | | | | | | |
| $H_2O_2$ | 74 | O (13s8p2d)/ [7s4p2d][h] | AHF | 150.8388 | 0.01 | 292 | 85849 | 71[p] |
| | | s: 6,2,1,1,1,1,1 | HF limit | $150.850 \pm 0.009$[m] | | | | |
| | | p: 4,2,1,1[k] | | | | | | |
| | | H (5s1p)/[3s1p][i] | | | | | | |
| | | s: 3,1,1[i] | | | | | | |

[a] Atomic function (AF) basis sets used are specified for each atom involved as follows: First two lines: number of basis orbitals, (GTOs)/[CGTOs]; second two lines: s grouping, p grouping.
[b] Total energy of the HF-procedure.
[c] Threshold parameter of the PERTCI method.
[d] Number of singly excited configurations involved.
[e] Number of doubly excited configurations involved.
[f] Correlation energy given as percentage of the total correlation energy. For the latter quantity, *see* Refs. n to p to this table.
[g] Von Niessen, W., Diercksen, G. H. F. and Cederbaum, L. S. (1977). *J. Chem. Phys., 67,* 4124.
[h] Van Duijneveldt, F. B. (1971). *IBM Research Rep.*, RJ 945.
[i] Karlström, G., Jönsson, B., Roos, B. O. and Siegbahn, P. E. M. (1978). *Theoret. Chim. Acta, 48,* 59.
[j] Huzinaga, S. (1965). *J. Chem. Phys., 42,* 1293.
[k] Lie, G. C. and Clementi, E. (1974). *J. Chem. Phys., 60,* 1275.
[ℓ] Christiansen, P. A. and McCullough Jr., E. A. (1977). *J. Chem. Phys., 67,* 1877.
[m] Hurley, A. C. (1976). *Introduction to Electron Theory*, pp. 289–290. London: Academic Press.
[n] Wilson, S. and Silver, D. M. (1977). *J. Chem. Phys., 67,* 1689.
[o] Tatewaki, H., Tanaka, K., Sasaki, F., Obara, S., Ohno, K. and Yoshimine, M. (1979). *Int. J. Quant. Chem., 15,* 533.
[p] McKelvey, J. M. and Streitwieser Jr., A. (1977). *J. Am. Chem. Soc., 99,* 7121.

1 mhartree above the HF energy) is plagued with the same error. This result emphasizes that the total AHF energy is of little use as a criterion for electron density accuracy. We revert to this point below, in connection with 4-31G+BF deformation densities.

Now let us turn to the correlation error. *Figure 1* presents maps of $\Delta\varrho_{\text{corr, AHF}}(\vec{r})$ for HC≡CH, $N_2$, $O_2$, and $F_2$ and *Figure 2* $\Delta\varrho_{\text{AHF CI}}(\vec{r})$ for the same molecules. The changes occurring in both series of functions are broadly understandable. Just as the correlation energy increases with the number of electrons, the correlation density gets more pronounced from HC≡CH to $F_2$. In HC≡CH the approximate minimum of $\Delta\varrho_{\text{corr}}(\vec{r})$ in the C≡C bond region is only $-0.02$ e/Å$^3$. It is systematically lowered from this value to $-0.06$ e/Å$^3$ in the N≡N bond of $N_2$, to $-0.08$ e/Å$^3$ in the O=O bond of $O_2$ and finally to $-0.1$ e/Å$^3$ in the F–F bond of $F_2$. Accordingly, electron correlation depletes electron density from the bonds, and similarly from the lone-pair regions. On the other hand, it accumulates this density near the nuclei. These results are in accordance with previous findings[24,48-61].

The changes that occur in the deformation densities $\Delta\varrho_{\text{AHF CI}}(\vec{r})$ when going from HC≡CH and $N_2$ to $F_2$ are plausible. Concerning the bond region there are mainly two effects determining the magnitude of the deformation density:

1. The accumulation of density due to overlap of the constituent atoms. This 'overlap effect' decreases with increasing bond distance[62] (i.e., is largest for $N_2$ and smallest for $F_2$).
2. The effect of subtracting *spherically averaged* atomic densities from the molecular densities.

For $O_2$ and especially for $F_2$, this means that relatively large atomic densities in the region of the $p_\sigma$ orbitals are subtracted, thus (partly) compensating the overlap effect. Clearly, the overlap effect can be made visible assuming non-spherical O and F atoms with one electron being in the $p_\sigma$ orbital[30]. It should be noted that the negative deformation density in the bond region of $F_2$ (*see Fig. 2d*)—a result which can be misunderstood—simply means that, in this region, there is less density in the molecule than in the artificial IAM molecule, and nothing more.

An important point concerns the magnitude of correlation densities relative to the corresponding deformation densities. Correlation densities are pronounced only near the nuclei (*Fig. 1*). These changes occur widely in regions where X-ray deformation densities cannot be determined accurately enough (within at least 0.3 Å from the nuclear centers). Eventually, electron diffraction deformation densities are better off in this respect, but unfortunately the ED method is hampered by other problems[27]. Therefore, these effects will hardly be seen in experiments at present. In the bond and lone-pair regions, the correlation densities are minor, and only in the O=O bond of $O_2$ and the F–F bond of $F_2$ would one line more occur in the deformation densities of *Figure 2* (*c and d*) if electron correlation were not included. These changes are again below that which can be detected with certainty in experiments (*see below*).

For $N_2$ and CO the basis set error and the correlation error in the deformation density are of comparable magnitude, but opposite in sign, in the bonding regions (the AHF density is too low by approximately 0.1 e/Å$^3$ relative to the HF density and the HF density is expected to be too high by at least 0.06 e/Å$^3$). Thus, in these two cases, the AHF density is more accurate than the AHF CI density near the midpoint of the bonds, due to a fortuitous compensating effect. It would be interesting to know whether the AHF density is generally too low near the midpoint

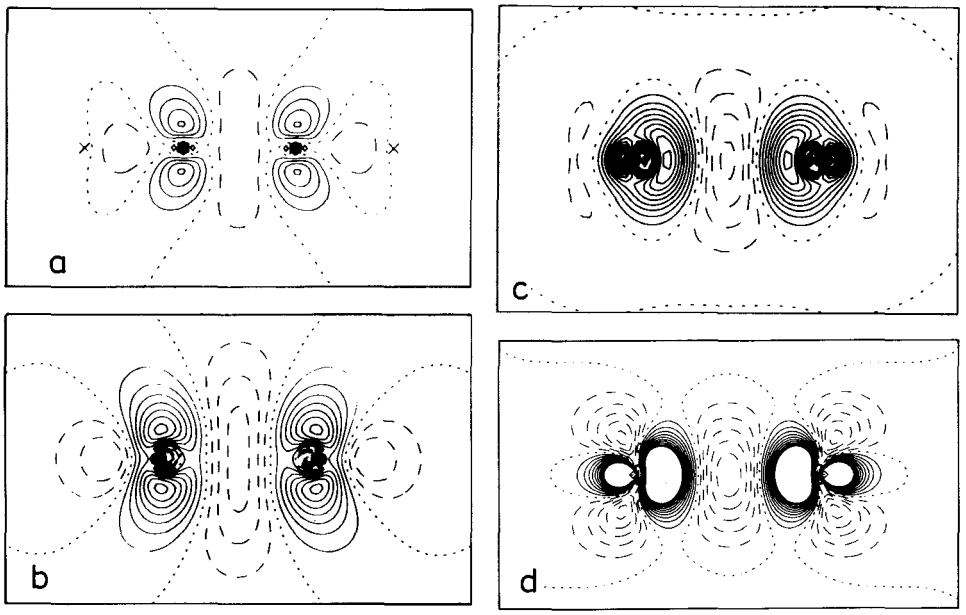


FIG. 1. Static correlation density $\Delta\varrho_{\text{corr, AHF}}(\vec{r})$ for (a) acetylene, (b) nitrogen, (c) oxygen, and (d) fluorine in the plane of the molecule. Contour line interval = 0.02 e/Å$^3$. Positive contours = full lines, negative contours = dashed lines, zero contour = dotted line.

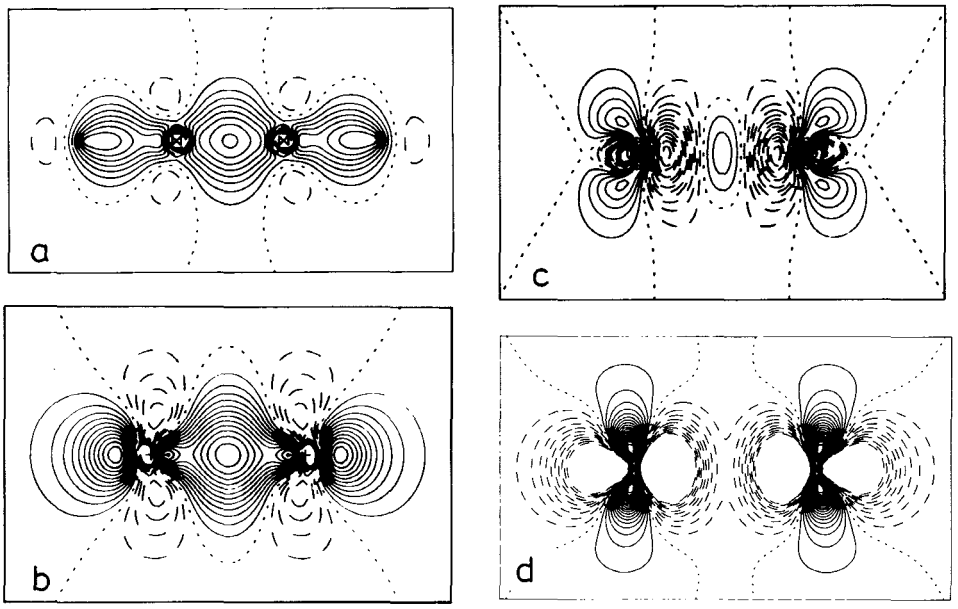


FIG. 2. Static deformation density $\Delta\varrho_{\text{AHF CI}}(\vec{r})$ of (a) acetylene, (b) nitrogen, (c) oxygen, and (d) fluorine in the plane of the molecule. Contour line interval = 0.1 e/Å$^3$. Sign convention of contour lines same as in *Figure 1*.

of a bond relative to the HF density. If this were so, the NHF densities would be very accurate in the bonds (note, however, *not* near the nuclei). As long as this is not known we must generally assume additivity of errors so that the total error in the static AHF deformation density near the midpoint of bonds could be roughly ±0.15 e/Å$^3$. However for $N_2$ and CO it is certain that the total deviation of the AHF CI density from the HF CI density is about −0.1 e/Å$^3$ and the deviation of the AHF from the HF CI density only about −0.05 e/Å$^3$. Furthermore note that thermal smearing would reduce all these errors by roughly 50%.

*We can state that we have presently to deal with errors of about ±0.1 e/Å$^3$ in the bonding regions of a molecule at rest and of about ±0.05 e/Å$^3$ in the same regions for a molecule moving in a crystal, in the best theoretical AHF CI deformation densities available.*

For $N_2$[63–65], $O_2$[65], HC≡CH[66], and $H_2O_2$[44] experimental deformation densities have been determined. They are contrasted with the AHF CI deformation densities in *Figures 3 to 6* and *Tables 2 to 5*.

For $N_2$ several ED densities have been produced[63–65]. The density of Ref. 63 is in error[65]. The densities of Refs. 64 (ED[b] of *Table 2*) and 65 (ED[c] and ED[d] of *Table 2*) are improved densities, but are still considered to be preliminary[65]. In *Figure 3*, only the latest $\Delta\varrho_{ED}(\vec{r})$ (ED[d] of *Table 2*) is confronted with $\Delta\varrho_{AHF\ CI}(\vec{r})$. Although the shape of $\Delta\varrho_{ED}(\vec{r})$ differs slightly from the shape of $\Delta\varrho_{AHF\ CI}(\vec{r})$ the overall agreement, and especially the agreement of the approximate maxima in the N≡N bond of both densities, is satisfactory. The agreement of the lone-pair maxima may be less satisfactory since the form of the ED map in the lone-pair region suggests that the computer may have arbitrarily stopped drawing at the 0.18 e/$a_0^3$ (1.2 e/Å$^3$) contour so that the maximum might be higher than suggested by the computer plot.

For $O_2$, two preliminary ED densities have been plotted[65]. Only the latest one is shown in *Figure 4*. Even if we admit that the AHF CI density maximum in the O=O bond may be underestimated by 0.02 e/$a_0^3$ (about 0.15 e/Å$^3$), in analogy to $N_2$, the ED density is clearly markedly in error in the bond. The same is true for the lone-

TABLE 2. Approximate deformation density maxima (e/Å$^3$) for nitrogen

| Method | N≡N | l.p.[a] |
|---|---|---|
| ED[b] | 1.1[e] | 1.2[e] |
| ED[c] | 0.8 | 0.9 |
| ED[d] | 1.2 | 1.2[f] |
| AHF CI | 1.2 | 1.1 |

[a] Lone-pair region.

[b] Bonham, R. A. and Fink, M. (1980). *Electron and Magnetization Densities in Molecules and Crystals* (ed. P. Becker), pp. 581–631. New York: Plenum Press.

[c] Fink, M. (January 1980). Personal communication.

[d] Fink, M. (September 1980). Personal communication.

[e] Values taken from *Figure 4* of Ref. b considering that the contour interval is 0.02 e/$a_0^3$ and not 0.01 e/$a_0^3$ as erroneously given in the figure caption: Fink, M. Personal communication.

[f] The form of the map of Ref. d in the lone-pair region suggests that the computer arbitrarily stopped drawing at the 0.18 e/$a_0^3$ (1.2 e/Å$^3$) contour so that the density maximum is likely to lie a few lines higher.

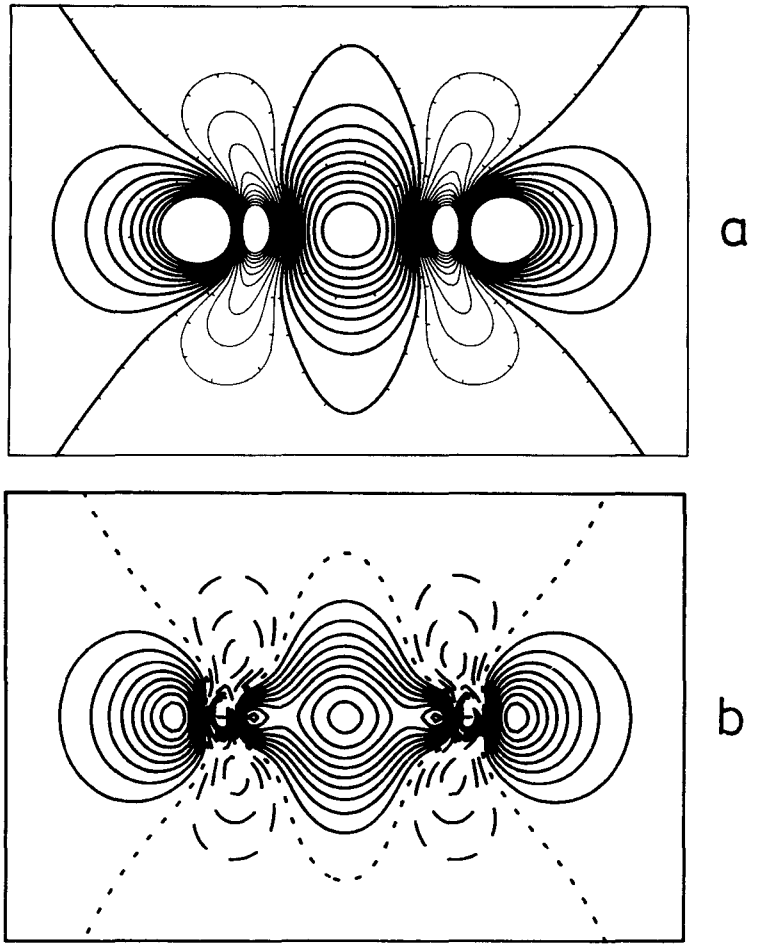


FIG. 3. Static deformation density of nitrogen in the plane of the molecule: (a) $\Delta\varrho_{ED}(\vec{r})$ of Ref. 65 ($ED^d$ of *Table 2*) and (b) $\Delta\varrho_{AHF\ CI}(\vec{r})$. Contour line interval = 0.02 $e/a_0^3$. Sign convention of contour lines in $\Delta\varrho_{ED}(\vec{r})$: zero and positive contours = thick lines, negative contours = fine lines. Sign convention of contour lines in $\Delta\varrho_{AHF\ CI}(\vec{r})$ same as in *Figure 1*.

pair region. The preceding $ED^b$ deformation density (cf. *Table 3*), on the contrary, underrated the O = O density, but overestimated the lone-pair density, too.

Although the ED densities of $N_2$ and $O_2$ are still preliminary, a comparison between these densities and our AHF CI densities appears meaningful. First, it demonstrates the difficulties of the electron diffraction method to produce correct deformation densities, and secondly it shows the importance of high-quality theoretical deformation densities (density standards) as a help in guiding experimental approaches.

For HC≡CH, X-ray M–A deformation densities have been published[66]. One of these densities ($M-A^{a,b}$ of *Table 4*) is contrasted with the thermally smeared AHF CI density in *Figure 5*.

TABLE 3. Approximate deformation density maxima (e/Å$^3$) for oxygen

| Method | O=O | l.p.[a] |
|---|---|---|
| ED[b] | 0.0 | 1.2[d] |
| ED[c] | 0.7 | 1.2[d] |
| AHF CI | 0.2 | 0.6 |

[a] Lone-pair region.
[b] Fink, M. (January 1980). Personal communication.
[c] Fink, M. (September 1980). Personal communication.
[d] The form of the map of Refs. b and c in the lone-pair region suggests that the computer arbitrarily stopped drawing at the 0.18 e/$a_0^3$ (1.2 e/Å$^3$) contour so that the density maximum is likely to be higher than the values given in the table.

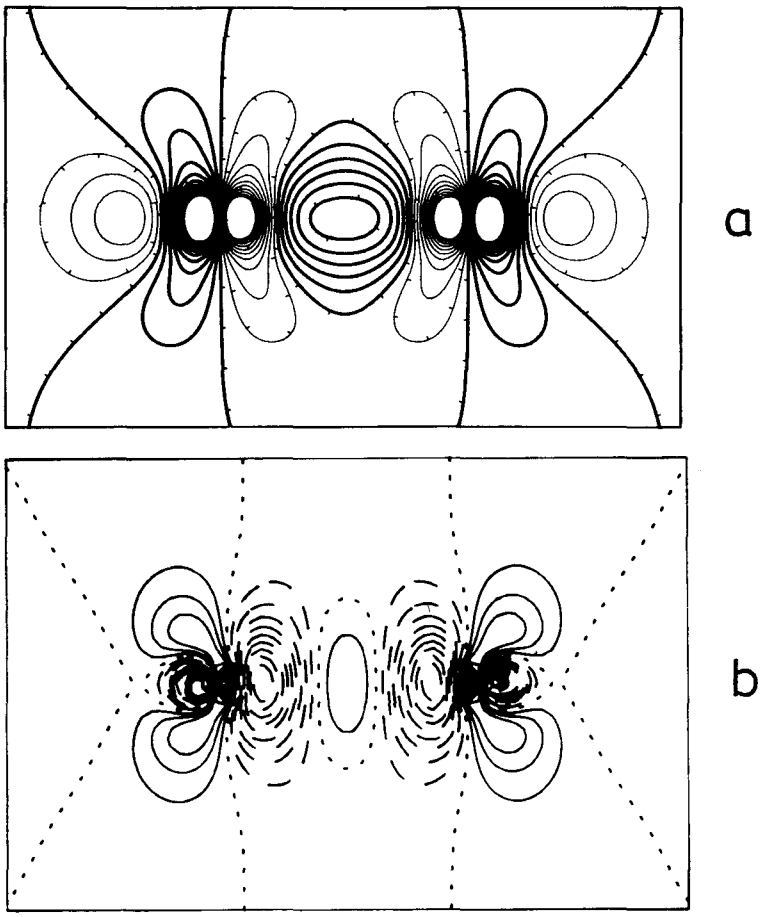


FIG. 4. Static deformation density of oxygen in the plane of the molecule: (a) $\Delta\varrho_{ED}(\vec{r})$ of Ref. 65 (ED[c] of *Table 3*) and (b) $\Delta\varrho_{AHF\ CI}(\vec{r})$. Contour line interval = 0.02 e/$a_0^3$. Sign convention of contour lines same as in *Figure 3*.

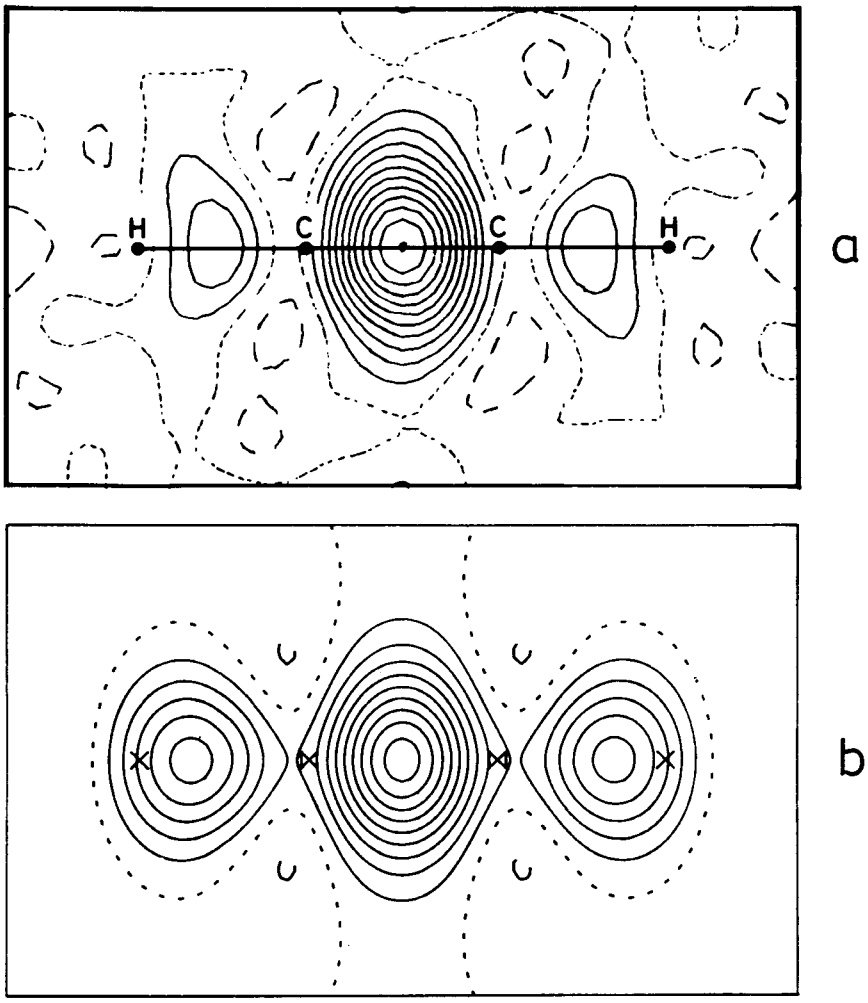


FIG. 5. Dynamic deformation density of acetylene in the plane of the molecule: (a) $\Delta\varrho_{M\text{-}A}(\vec{r})$ of Ref. 66 (M–A[a,b] of *Table 4*) and $\Delta\varrho_{AHF\ CI}(\vec{r})$. Contour line interval = 0.05 e/Å$^3$. Sign convention of contour lines same as in *Figure 1*.

TABLE 4. Approximate deformation density maxima (e/Å$^3$) for acetylene at 141 K

| Method | C≡C | C–H |
|---|---|---|
| M–A[a,b] | 0.50 | 0.10 |
| M–A[a,c] | 0.70 | 0.15 |
| AHF[a] | 0.50 | 0.10 |
| AHF CI | 0.45 | 0.25 |

[a] Van Nes, G. J. H. and van Bolhuis, F. (1979). *Acta Cryst., B35*, 2580.
[b] $^3$P scattering factor for carbon and f(H) scattering factor for hydrogen, cf. Ref. a.
[c] $\xi$ scattering factors, cf. Ref. a.

Thermal smearing is based on the following data: $\sin\theta/\lambda = 0.8$ Å$^{-1}$; pseudo-unit cell dimensions: $|\vec{a}| = 4$ Å, $|\vec{b}| = 4$ Å, and $|\vec{c}| = 6$ Å; the $U_k$ as averaged from refinements A3 and C5 of Ref. 66; the $U_{kl}$ of the interatomic $\phi_\mu\phi_\nu$ ($\mu$ on atom $k$, $\nu$ on atom $l$) density units from $(U_k + U_l)/2$.

The agreement between the experimental and theoretical densities in the C≡C bond is satisfactory (difference in the bond maxima 0.05 e/Å$^3$) and slightly less satisfactory in the C–H bond (discrepancy between theory and experiment 0.15 e/Å$^3$). This discrepancy is slightly higher than expected from the error in our theoretical dynamic deformation densities (about ±0.07 e/Å$^3$ or less, near the midpoint of a bond), according to the above considerations. The X-ray experiment on HC≡CH is plagued with strong thermal motion, even at 141 K. Since our static AHF deformation density and that of Ref. 66 agree, it was supposed that the aforementioned discrepancy could also be due to our thermal averaging procedure[67]. At present, there is no further evidence to examine this point. On the whole—and this will be evident from comparisons presented later in the review—agreement between an experimental X-ray deformation density and our theoretical deformation density within ±0.1 or ±0.15 e/Å$^3$ is very good, in view of possible systematic errors in the experiments (cf. also Ref. 27).

For $H_2O_2$, X–X and X–N deformation densities are available[44]. In *Figure 6* $\Delta\varrho_{X\text{-}N}(\vec{r})$ is confronted with the thermal averaged $\Delta\varrho_{AHF\ CI}(\vec{r})$. *Table 5* lists the approximate deformation density maxima in the respective bonds and lone pairs.

Thermal smearing was performed on the basis of the following data: $\sin\theta/\lambda = 0.9$ Å$^{-1}$; pseudo-unit cell dimensions: $|\vec{a}| = 5$ Å, $|\vec{b}| = 5$ Å, and $|\vec{c}| = 7$ Å; the $U_k$ neutron data from Ref. 44; the $U_{kl}$ from $(U_k + U_l)/2$.

The maps and data show that agreement between experiment and theory is quite good, except for the differing l.p.[b] (cf. *Table 5*) lone-pair maximum. As contrasted with $\Delta\varrho_{AHF\ CI}(\vec{r})$, the X–N l.p.[b] maximum is clearly in error. In agreement with the theoretical density, practically equal lone-pair peaks would be expected for the section shown, simply from the geometrical data. Interestingly, the difference between both peaks is less pronounced in the X–X density. Model calculations concerning the question whether this defect of the X–N density is due to using the phases from a conventional refinement (phase error) in the experimental Fourier difference syntheses are in progress[68]. *Figure 7* adds maps of the static $\Delta\varrho_{AHF}(\vec{r})$ and $\Delta\varrho_{corr,\ AHF}(\vec{r})$ densities. It is obvious that the effects of electron correlation in bonding and lone-pair regions are minor.

The AHF and correlation densities of CO and $H_2O$ are discussed in the next section. Experimental densities are not available.

TABLE 5. Approximate deformation density maxima (e/Å$^3$) for hydrogen peroxide at 110 K

| Method | O–O | O–H | l.p.[a] | l.p.[b] | l.p.[c] |
|---|---|---|---|---|---|
| X–X[d] | 0.1 | 0.3 | 0.5 | 0.8 | 0.7 |
| X–N[d] | 0.0 | 0.4 | 0.5 | 0.9 | 0.6 |
| AHF CI | 0.0 | 0.4 | 0.4 | 0.6 | 0.6 |

[a] Lone pair on the oxygen atom that is directed towards H(+1.4), cf. *Figure 6a* of the present paper.

[b] Lone pair on the oxygen atom that is directed towards H(−0.8), cf. *Figure 6a* of the present paper.

[c] Other lone pair on the same oxygen as in Ref. b.

[d] Savariault, J.-M. and Lehmann, M. S. (1980). *J. Am. Chem. Soc., 102,* 1298.

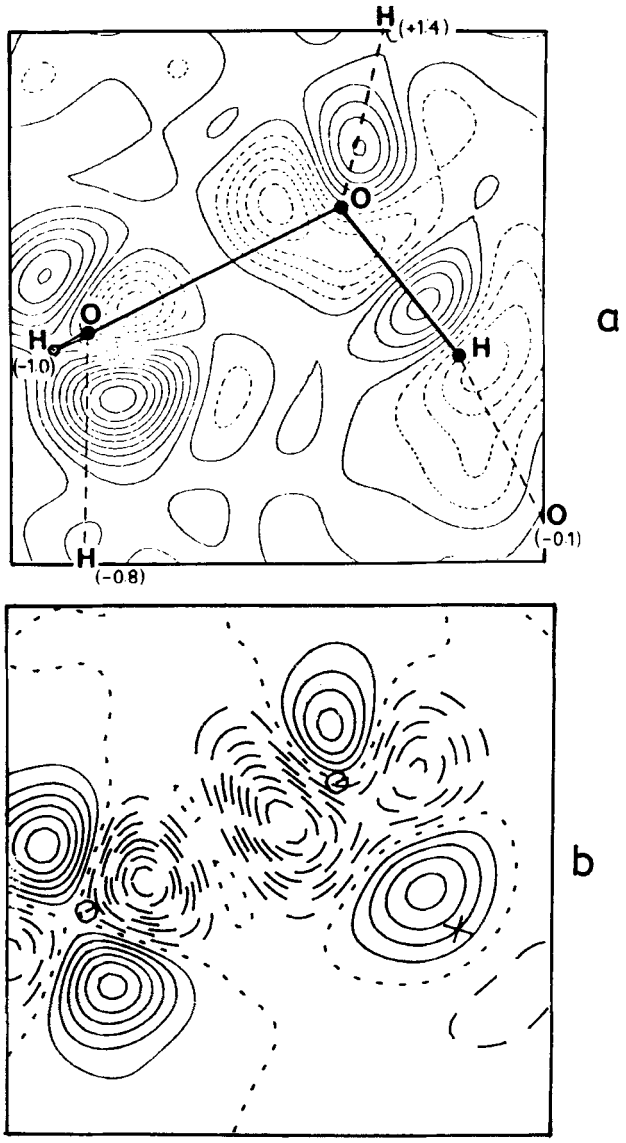


FIG. 6. Dynamic deformation density of hydrogen peroxide in the OOH plane: (a) $\Delta\varrho_{X\text{-}N}(\vec{r})$ of Ref. 44 (X–N$^d$ of *Table 5*) and (b) $\Delta\varrho_{AHF\ CI}(\vec{r})$. Contour line interval = 0.1 e/Å$^3$. Sign convention of contour lines in $\Delta\varrho_{X\text{-}N}(\vec{r})$: zero and positive contours = full lines, negative contours = dashed lines. Sign convention of contour lines in $\Delta\varrho_{AHF\ CI}(\vec{r})$ same as in *Figure 1*.

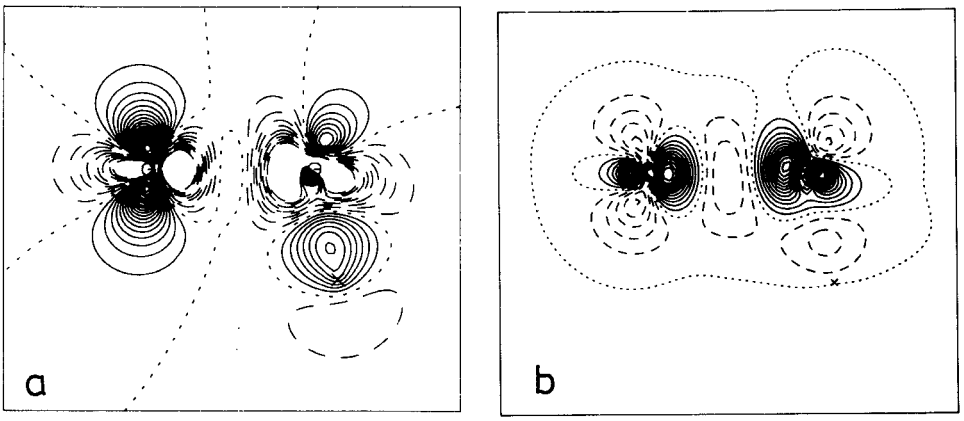


FIG. 7. (a) Static deformation density $\Delta\varrho_{AHF}(\vec{r})$ and (b) correlation density $\Delta\varrho_{corr,AHF}(\vec{r})$ of hydrogen peroxide in the OOH plane. Contour line interval = 0.1 e/Å$^3$ in (a) and 0.02 e/Å$^3$ in (b). Sign convention of contour lines same as in *Figure 1.*



### *3.2 Small molecules: 4-31G + BF deformation densities versus deformation density standards*

Bond functions (BFs) or bond polarization functions (BPs) have been in use in quantum-chemical *ab initio* calculations for about 25 years[22,23,25b,57,62,69-89]. In 1977, we introduced bond functions into deformation density calculations and combined the well known 4-31G basis set[90-93] with BFs. This was a very fortunate choice as we demonstrate below.

In addition to the molecules $N_2$, $O_2$, $F_2$, CO, $H_2O$, HC≡CH and $H_2O_2$ that were considered in the foregoing section, we include $CN^-$, HCN, $SCN^-$, $C_2H_4$, and $C_2N_2$ in the present comparisons. Experimental geometries have been used: $CN^-$[94] R = 1.153 Å, HCN[95] R(CN) = 1.155 Å, R(CH) = 1.063 Å, $SCN^-$[96] R(CN) = 1.217 Å, R(CS) = 1.561 Å, $C_2H_4$[97] R(CC) = 1.337 Å, R(CH) = 1.086 Å, ∢ CCH = 121.3°, $C_2N_2$[98] R(CC) = 1.380 Å, R(CN) = 1.157 Å.

Appropriate BFs to be used with the 4-31G basis set are specified in *Table 6.* One primitive GTO s function and one set of primitive GTO p functions are placed at the midpoint of each bond considered, except for the hydrogen bonds, where only one s function was used. The exponents of all BFs were determined by optimizing the total energy of the molecules listed in *Table 6.* During the optimization process, BFs were placed only in the bonds under consideration and not in the others.

Before *Table 6* was established, we applied BFs which were defined in a different way. At first, we did not differentiate between single, double, triple or aromatic bonds. Instead we used just one set for each bond, for C–C s 1.4, p 0.5, N–N s 1.7, p 0.85, C–N s 1.55, p 0.65, C–O s 1.35, p 0.8, C–S s 0.5, p 0.5. The C–C values were taken from Ref. 99; they were optimized for $C_2H_4$ using an AHF basis set somewhat different from the 4-31G set. The N–N, C–O, and C–S values are identical with the values for N≡N, C = O, and C = S of *Table 6.* The C–N values given are the mean of the respective C–C and N–N values.

In two cases, the calculation of the deformation densities of $NaN_3$ and NaSCN under the influence of the crystal environment, only two p functions were used in the

TABLE 6. Bond functions

| Bond | BF[a] | Molecule[b] |
|---|---|---|
| C - C | s 0.9 p 0.85 | $H_3C-CH_3$ |
| C = C | s 1.45 p 0.9 | $H_2C=CH_2$ |
| C ≡ C | s 1.65 p 1.0 | HC ≡ CH |
| C ⋍ C | s 1.2 p 0.9 | $H_2C$ ⋍ $CH_2$[c] |
| N - N | s 0.7 p 0.4 | $H_2N-NH_2$ |
| N = N | s 1.0 p 0.65 | HN = NH |
| N ≡ N | s 1.7 p 0.85 | N ≡ N |
| O - O | s 0.8 p 0.6 | HO-OH |
| O = O | s 1.0 p 0.8 | O = O[d] |
| F-F | s 1.0 p 1.0 | F-F |
| C - N | s 0.8 p 0.8 | $H_3C-NH_2$ |
| C = N | s 1.2 p 0.8 | $H_2C=NH$ |
| C ≡ N | s 1.7 p 0.9 | HC ≡ N |
| C ⋍ N | s 1.1 p 0.75 | $H_2C$ ⋍ NH[e] |
| C - O | s 0.9 p 0.7 | $H_3C-OH$ |
| C = O | s 1.35 p 0.8 | $H_2C=O$ |
| C - F | s 1.0 p 0.8 | $H_3C-F$ |
| N - O | s 0.8 p 0.6 | $H_2N-OH$ |
| N = O | s 1.1 p 0.7 | $[ON=O]^+$ |
| N ≡ O | s 1.8 p 0.8 | $[N\equiv O]^+$ |
| C - H | s 1.25 | $H_3C-H$ |
| N - H | s 1.0 | $H_2N-H$ |
| O - H | s 1.15 | HO-H |
| F - H | s 1.25 | F-H |
| P - P | s 0.35 p 0.4 | $H_2P-PH_2$ |
| S - S | s 0.4 p 0.3 | S = S[d,f] |
| Cl-Cl | s 0.5 p 0.5 | Cl-Cl |
| C - P | s 0.5 p 0.55 | $H_3C-PH_2$ |
| C = P | s 0.55 p 0.5 | $H_2C=PH$ |
| C ≡ P | s 0.6 p 0.55 | HC ≡ P |
| C ⋍ P | s 0.5 p 0.5 | $H_2C$ ⋍ PH[g] |
| C - S | s 0.5 p 0.6 | $H_3C-SH$ |
| C = S | s 0.5 p 0.5 | $H_2C=S$ |
| C - Cl | s 0.6 p 0.6 | $H_3C-Cl$ |
| P - H | s 0.5 | $H_2P-H$ |
| S - H | s 0.6 | HS-H |
| Cl-H | s 0.65 | Cl-H |
| S - O | s 0.7 p 0.6 | S = O[d,f] |

[a] Bond functions (BF) are specified as follows: type of BF (s or p) followed by its exponential parameter.

[b] Molecule for which the BF exponential parameters are optimized. BFs are placed in the midpoint of the respective bonds, only. Experimental geometries are used throughout; for further details, *see* Refs. c, e, f, and g to this table.

[c] Geometry adapted to benzene.

[d] Molecule in its lowest triplet state.

[e] Geometry adapted to pyridine.

[f] Bond length as in $Na_2S_2O_6$.

[g] Geometry adapted to phosphorine.

N–N, C–S, and C–N bonds. The exponents used were those specified in the preceding paragraph.

Amongst the molecules considered in the present section, the 4–31G + BF calculations are based on the BFs of *Table 6* for $N_2$, $O_2$, $F_2$, $H_2O$, and $H_2O_2$, and for the rest of the molecules on the slightly different set as specified above. Test calculations have shown that both sets of BFs lead to almost the same deformation densities.

*Table 7* lists the approximate deformation density maxima in the bonding and lone-pair regions of $\Delta\varrho_{4\text{–}31G+BF}(\vec{r})$ and $\Delta\varrho_{NHF}(\vec{r})$. As can be seen, the agreement between both sets of data is excellent. Normally, the deviations are ±0.1 e/Å$^3$ or less and exceed ±0.1 e/Å$^3$ only in the lone-pair region of $F_2$ and in the O–O bond of $H_2O_2$. Thus we can state: *Bond and lone-pair maxima are described by the 4–31G + BF basis set in almost NHF quality. The mean deviation between both sorts of values is less than ±0.1 e/Å$^3$.*

As *Figures 8 and 9* demonstrate for the two examples of non-polar molecules, $N_2$ and HC ≡ CH, and *Figures 10 and 11* for two examples of polar molecules, namely CO and $H_2O$, there is impressive agreement between the whole shape of 4–31G + BF and NHF deformation densities.

Two remarks are to be added. First, the excellent agreement between the 4–31G + BF and NHF deformation densities is especially notable in view of the rather bad AHF energy obtained with the 4–31G + BF basis set. Secondly, the bond functions are quite essential for the quality of the 4–31G + BF deformation densities; omitting the BFs leads to maxima in the bonding regions being too low by about 0.1 to 0.2 e/Å$^3$ (the lone-pair peaks are hardly influenced, however).

*Figures 12 to 15*, moreover, testify, for the same choice of molecules, that $\Delta\varrho_{corr,\ 4\text{–}31G+BF}(\vec{r})$ also nearly perfectly mimics the very elaborate $\Delta\varrho_{corr,\ NHF}(\vec{r})$ densities. The total number of SECs and DECs amount, for 4–31G + BF calculations, to: $N_2$ 917, HC ≡ CH 2003, CO 1825, and $H_2O$ 434, in comparison to the much larger numbers of configurations to be dealt with in the high-quality calculations of the preceding section (cf. *Table 1*). It should be noted that the 4–31G + BF CI calculations are SELCI calculations (including all SECs and DECs) and thus avoid perturbation corrections. It is even more interesting to note that it is unnecessary to include all the DECs in a 4–31G + BF calculation; it is sufficient to take all the SECs and only the 10–20% most efficient DECs to get correlation densities that are very similar to the correlation densities represented in *Figures 12 to 15*.

The aforementioned data and facts verify that the 4–31G + BF basis set is the basis set of choice for predictions of deformation densities. The 4–31G + BF AHF and AHF CI deformation densities are practically identical with NHF and NHF CI densities and much more economically obtained than the latter, as the following representative computation times exemplify: $N_2$ AHF of *Table 1* = 6.5 h, AHF PERTCI = 19 h; 4–31G + BF = 0.04 h, 4–31G + BF SELCI = 0.27 h, CH ≡ CH AHF of *Table 1* = 4.7 h, AHF PERTCI = 23 h; 4–31G + BF = 0.16 h, 4–31G + BF SELCI = 0.44 h, CO AHF of *Table 1* = 3.3 h, AHF PERTCI = 21 h; 4–31G + BF = 0.09 h, 4–31G + BF SELCI = 0.9 h, $H_2O$ AHF of *Table 1* = 0.8 h, AHF PERTCI = 2.5 h; 4–31G + BF = 0.04 h, 4–31G + BF SELCI = 0.09 h (all computation times refer to a Telefunken TR 440 using the POLYATOM and PERTCI program systems).

With these results the 4–31G + BF basis set strongly recommends itself for the calculation of deformation densities of larger molecules. Since the correlation corrections to the deformation densities appear to be low and since there is some chance that AHF densities may be less in error in bonds than AHF CI densities (cf. preceding section) we feel justified to make comparisons of experimental with theoretical densities of large molecules on the basis of AHF calculations alone.

TABLE 7. Approximate deformation density maxima in $\Delta\varrho_{AHF}$

| Molecule | Region | 4-31G + BF | NHF[a,b] | Unit[c] | Basis set[d] |
|---|---|---|---|---|---|
| $N_2$ | N≡N | 0.20 | 0.18[f] | $e/a_o^3$ | STO, f[n] |
| | 1.p.[e] | 0.16 | 0.14[f] | | |
| $O_2$ | O=O | 0.35 | 0.35[g] | $e/Å^3$ | CGTO, d[g] |
| | 1.p.[e] | 0.40 | 0.40[g] | | |
| $F_2$ | F-F | 0.0 | −0.1[h] | $e/Å^3$ | CGTO, d[g] |
| | 1.p. | 1.9 | 2.1[h] | | |
| CO | C≡O | 0.150 | 0.150[i] | $e/a_o^3$ | STO, f[n] |
| | 1.p.(C)[e] | 0.100 | 0.100[i] | | |
| | 1.p.(O)[e] | 0.100 | 0.100[i] | | |
| $CN^-$ | C≡N | 0.175 | 0.150[j] | $e/a_o^3$ | STO, d[o] |
| | 1.p.(C)[e] | 0.100 | 0.100[j] | | |
| | 1.p.(N)[e] | 0.125 | 0.125[j] | | |
| HCN | C≡N | 1.1 | 1.0[k] | $e/Å^3$ | STO, f;d[n] |
| | C-H | 0.7 | 0.7[k] | | |
| | 1.p.[e] | 1.0 | 1.0[k] | | |
| $H_2O$ | O-H | 0.7 | 0.7[g] | $e/Å^3$ | CGTO, d;p[g] |
| | 1.p.[e] | 0.8 | 0.7[g] | | |
| $SCN^-$ | S-C | 0.6 | 0.6[ℓ] | $e/Å^3$ | STO, f[n] |
| | C-N | 0.9 | 0.8[ℓ] | | |
| | 1.p.(S)[e] | 0.1 | 0.1[ℓ] | | |
| | 1.p.(N)[e] | 0.7 | 0.7[ℓ] | | |
| $C_2H_2$ | C≡C | 0.8 | 0.8[k] | $e/Å^3$ | STO, f;d[n] |
| | C-H | 0.7 | 0.8[k] | | |
| $C_2H_4$ | C=C | 0.80 | 0.75[m] | $e/Å^3$ | CGTO, d;p[p] |
| | C-H | 0.75 | 0.80[m] | | |
| $H_2O_2$ | O-O | 0.2 | 0.0[g] | $e/Å^3$ | CGTO, d;p[g] |
| | O-H | 0.7 | 0.7[g] | | |
| | 1.p.[e] | 1.9 | 1.9[g] | | |
| $C_2N_2$ | C≡N | 1.1 | 1.0[k] | $e/Å^3$ | STO, f[n] |
| | C-C | 0.6 | 0.6[k] | | |
| | 1.p.[e] | 1.1 | 1.1[k] | | |

[a] The highest contour line that can be read from literature maps is given.
[b] Values taken from the quoted NHF plots.
[c] Conversion factor: $1\ e/a_o^3 = 6.74873\ e/Å^3$.
[d] Basis set is specified as follows: type of AFs used, polarization functions on heavy atoms included up to d or f; polarization functions on hydrogen atoms up to p or d.
[e] Lone pair.
[f] Smith, P. R. and Richardson, J. W. (1967). *J. Phys. Chem., 71,* 924.
[g] Present work.
[h] Ransil, B. J. and Sinai, J. J. (1967). *J. Chem. Phys., 46,* 4050.
[i] De With, G. and Feil, D. (1975). *Chem. Phys. Lett., 30,* 279.
[j] Bats, J. W. and Feil, D. (1977). *Chem. Phys., 26,* 79.
[k] Hirshfeld, F. L. (1971). *Acta Cryst., B27,* 769.
[ℓ] Bats, J. W., Coppens, P. and Kivick, A. (1977). *Acta Cryst., B33,* 1534.
[m] Van Nes, G. J. H. (1978). Doctoral Dissertation, Groningen.
[n] McLean, A. D. and Yoshimine, M. (1967). *Tables of Linear Molecule Wave Functions.* IBM.
[o] Bonaccorsi, R., Petrongolo, C., Scrocco, E. and Tomasi, J. (1969). *Chem. Phys. Lett., 3,* 473.
[p] Van Nes, G. J. H. and Vos, A. (1979). *Acta Cryst., B35,* 2593.

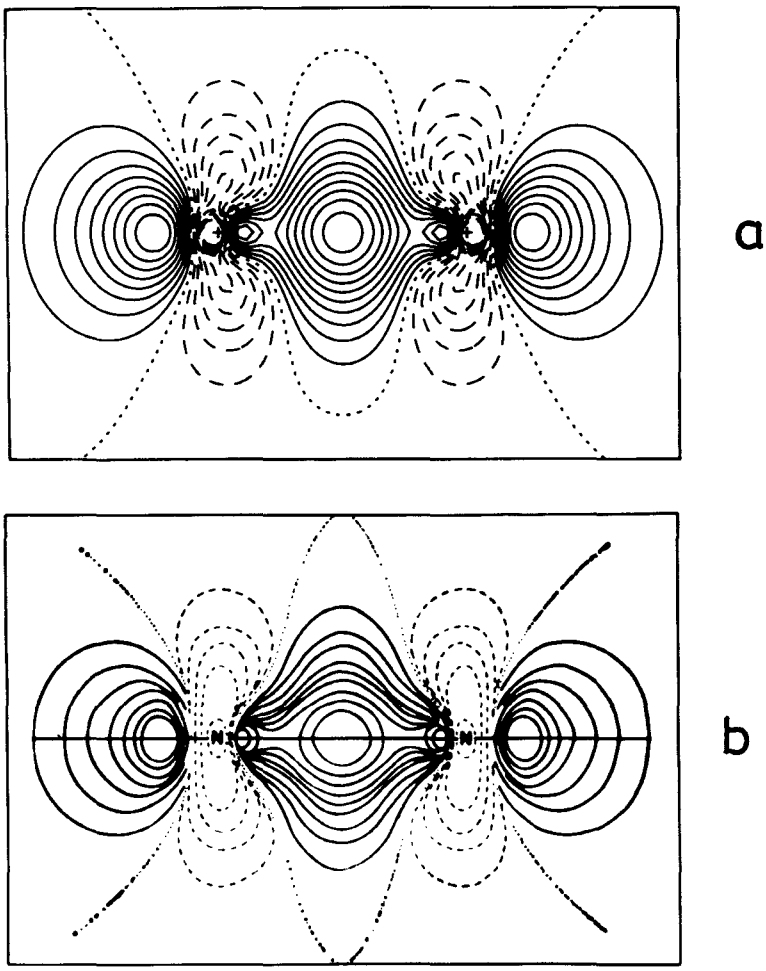


FIG. 8. Static deformation density of nitrogen in the plane of the molecule: (a) $\Delta\varrho_{4\text{-}31G+BF}(\vec{r})$ and (b) $\Delta\varrho_{NHF}(\vec{r})$ of Refs. n and f of *Table 7*. Contour line interval = 0.02 e/$a_o^3$. Sign convention of contour lines same as in *Figure 1*.

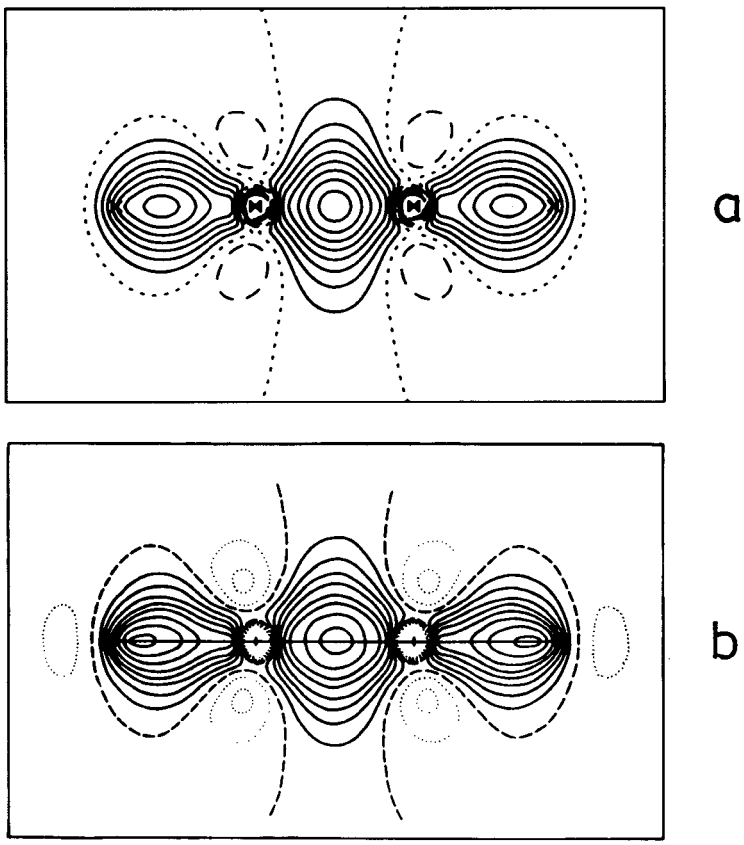


FIG. 9. Static deformation density of acetylene in the plane of the molecule: (a) $\Delta\varrho_{4\text{-}31G+BF}(\vec{r})$ and (b) $\Delta\varrho_{NHF}(\vec{r})$ of Refs. n and k of *Table 7*. Contour line interval = 0.1 e/Å$^3$. Sign convention of contour lines in $\Delta\varrho_{4\text{-}31G+BF}(\vec{r})$ same as in *Figure 1*. Sign convention of contour lines in $\Delta\varrho_{NHF}(\vec{r})$: positive contours = full lines, negative contours = dotted lines, zero contour = dashed line.

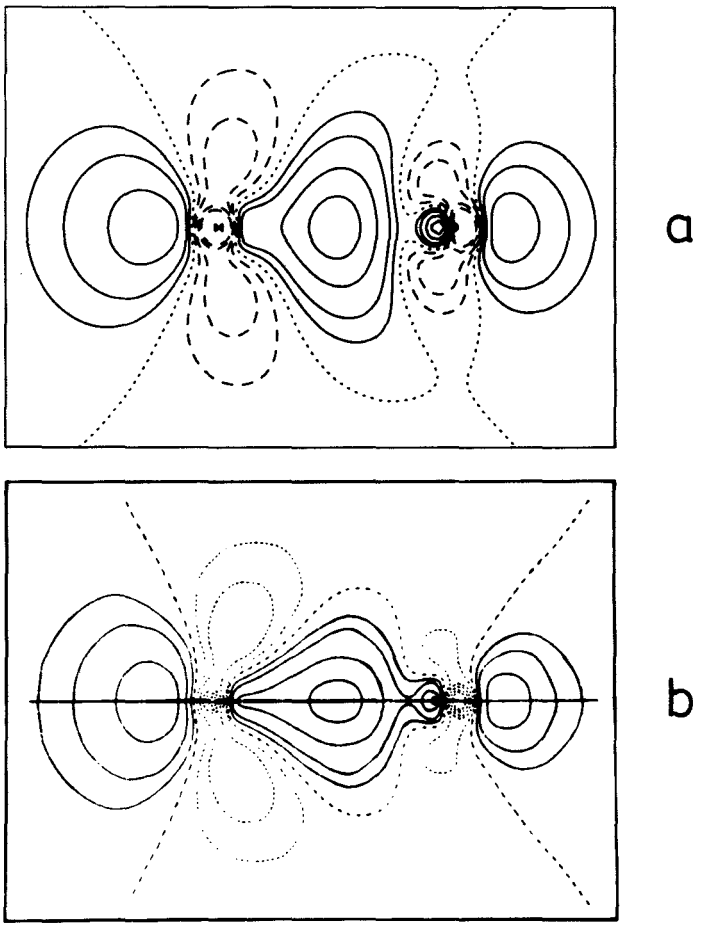


FIG. 10. Static deformation density of carbon monoxide in the plane of the molecule. C atom on the left. (a) $\Delta\varrho_{4\text{-}31G+BF}(\vec{r})$ and (b) $\Delta\varrho_{NHF}(\vec{r})$ of Refs. n and i of *Table 7*. Contour lines at 0, ±0.025, ±0.050, ±0.100, and ±0.150 e/$a_0^3$. Sign convention of contour lines in $\Delta\varrho_{4\text{-}31G+BF}(\vec{r})$ same as in *Figure 1*. Sign convention of contour lines in $\Delta\varrho_{NHF}(\vec{r})$: positive contours = full lines, negative contours = dotted lines, zero contour = dashed line.

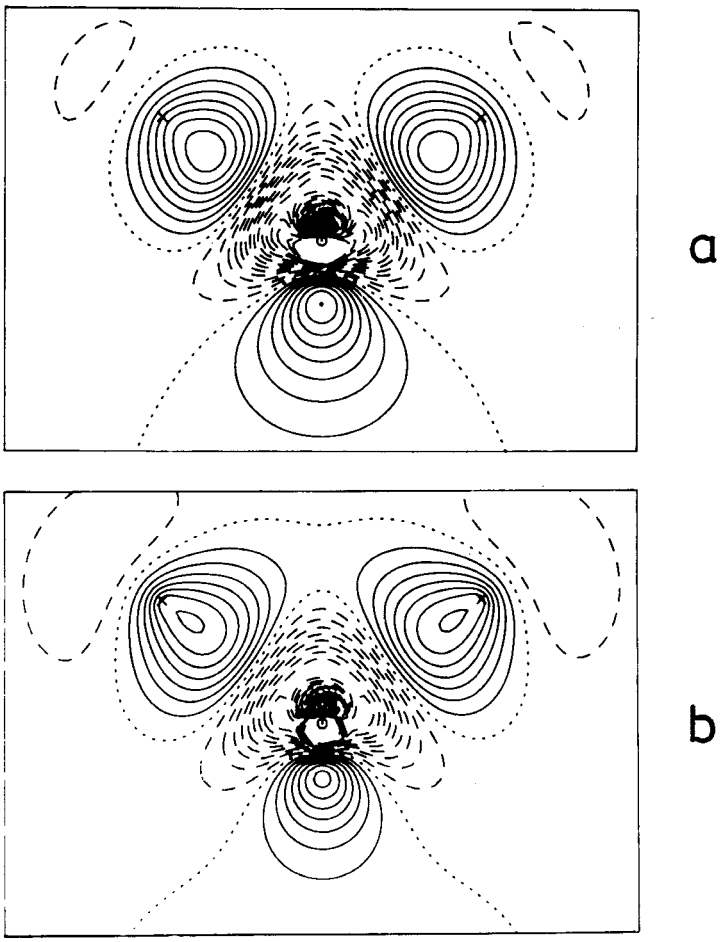


FIG. 11. Static deformation density of the water molecule in the plane of the molecule. O atom in the lower part and H atoms in the upper part of the maps. (a) $\Delta\varrho_{4\text{-}31G+BF}(\vec{r})$ and (b) $\Delta\varrho_{NHF}(\vec{r})$ of the present work (cf. *Table 1*). Contour line interval = 0.1 e/Å$^3$. Sign convention of contour lines same as in *Figure 1*.

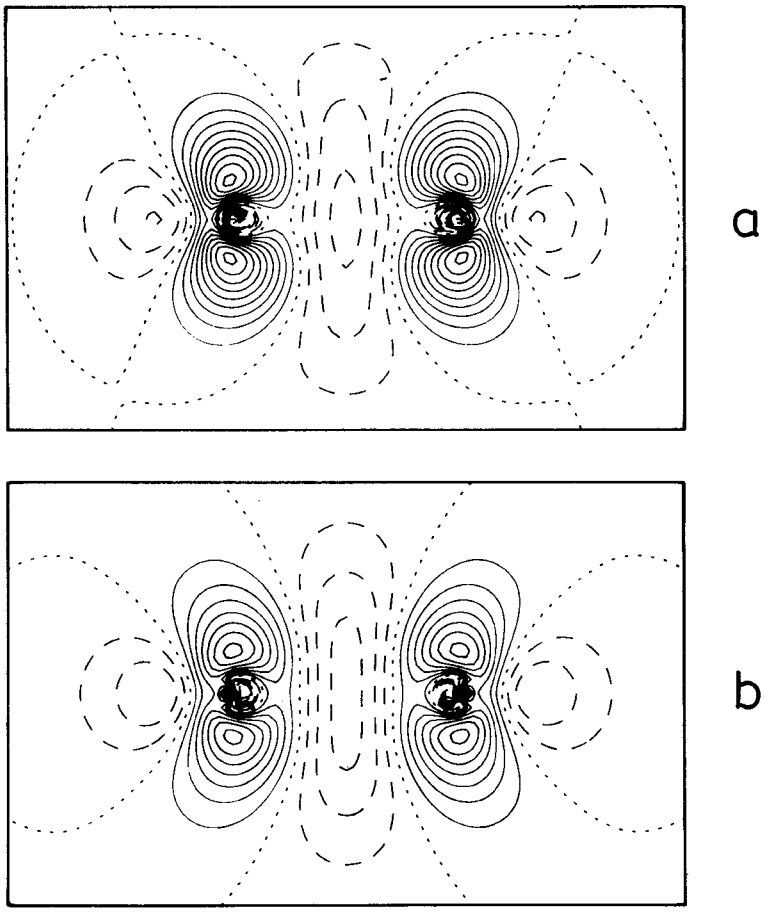


FIG. 12. Static correlation density of nitrogen in the plane of the molecule. (a) $\Delta\varrho_{\text{corr, 4-31G+BF}}(\vec{r})$ and (b) $\Delta\varrho_{\text{corr, NHF}}(\vec{r})$ of present work (cf. *Table I*). Contour line interval = 0.02 e/Å$^3$. Sign convention of contour lines same as in *Figure 1*.

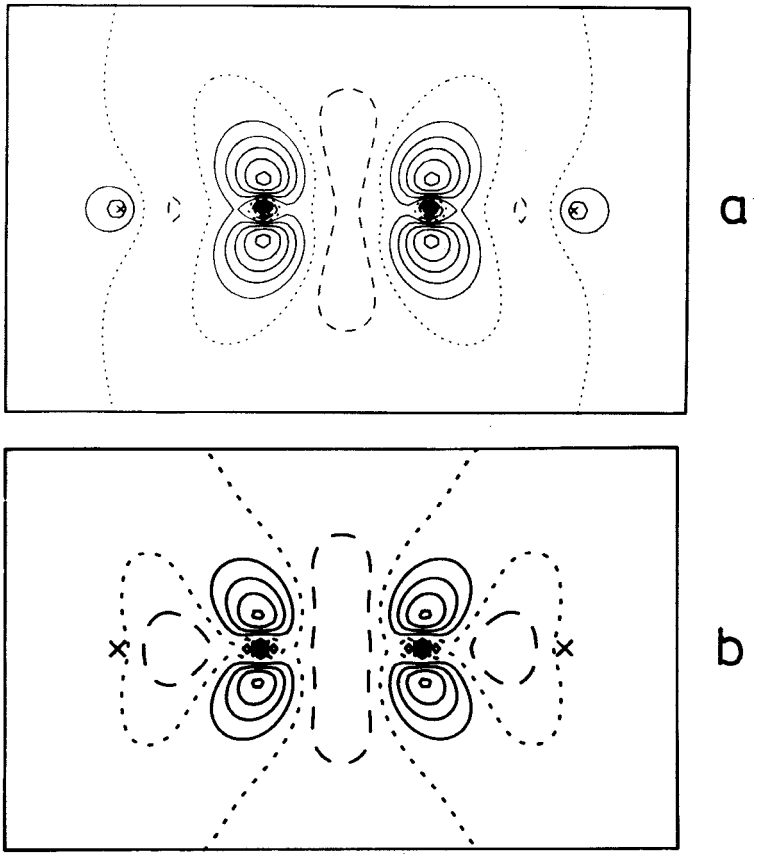


FIG. 13. Static correlation density of acetylene in the plane of the molecule: (a) $\Delta\varrho_{\text{corr, 4-31G+BF}}(\vec{r})$ and (b) $\Delta\varrho_{\text{corr, NHF}}(\vec{r})$ of the present work (cf. *Table 1*). Contour line interval = 0.02 e/Å$^3$. Sign convention of the contour lines same as in *Figure 1*.

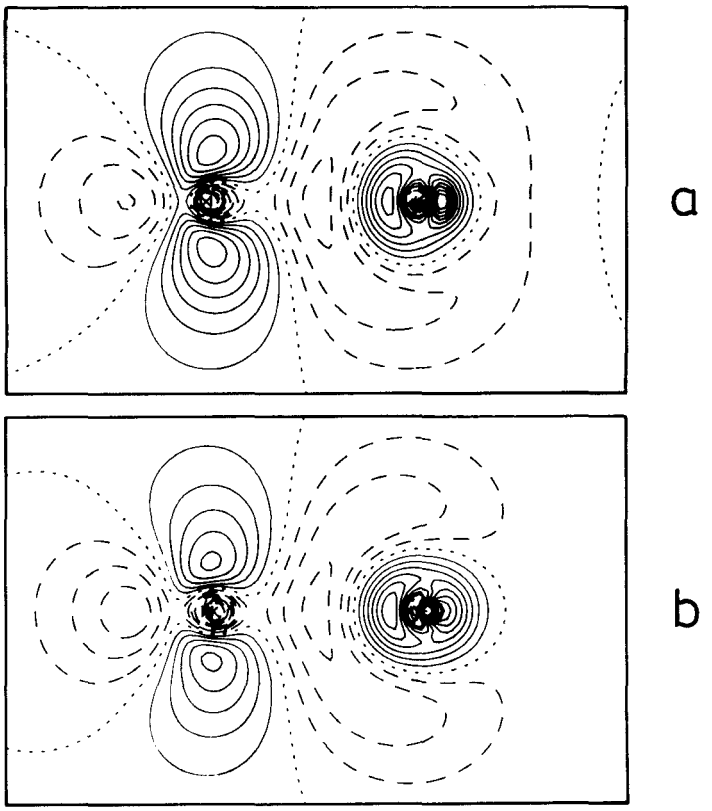


FIG. 14. Static correlation density of carbon monoxide in the plane of the molecule. C atom on the left. (a) $\Delta\varrho_{\text{corr, 4-31G+BF}}(\vec{r})$ and (b) $\Delta\varrho_{\text{corr, NHF}}(\vec{r})$ of the present work (cf. *Table 1*). Contour line interval = 0.02 e/Å$^3$. Sign convention of contour lines same as in *Figure 1*.

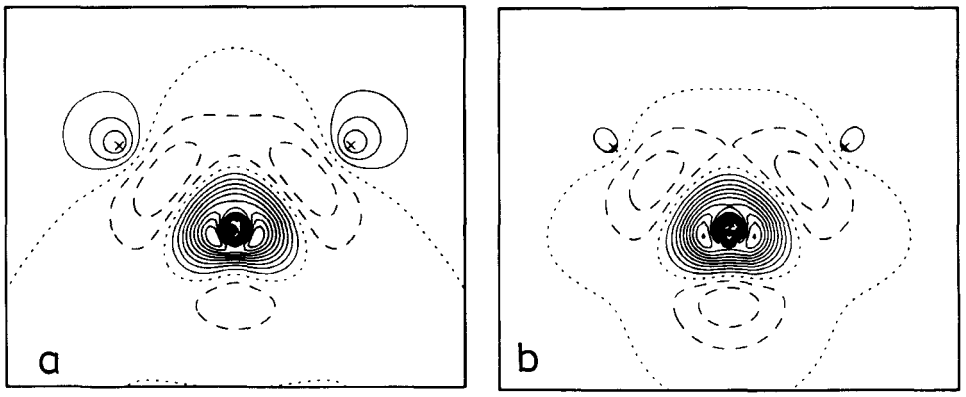


FIG. 15. Static correlation density of the water molecule in the plane of the molecule: O atom in the lower part, and H atoms in the upper part of the maps. (a) $\Delta\varrho_{\text{corr, 4-31G+BF}}(\vec{r})$ and (b) $\Delta\varrho_{\text{corr, NHF}}(\vec{r})$ of the present work (cf. *Table 1*). Contour line interval = 0.02 e/Å$^3$. Sign convention of contour lines same as in *Figure 1*.

### *3.3 Large molecules: experimental versus 4–31G + BF AHF deformation densities*

As representative examples we select cyanuric acid, tetracyanoethylene, formamide, oxalic acid, urea and thiourea.

The 4–31G + BF calculations of cyanuric acid are based on the neutron positional parameters[100] and the BF exponents specified

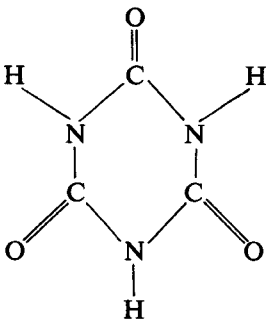

in the text of the preceding section. For the thermal smearing procedure, the following data are used: $\sin\theta/\lambda = 0.8$ Å$^{-1}$; pseudo-unit cell dimensions: $|\vec{a}| = 7$ Å, $|\vec{b}| = 5$ Å and $|\vec{c}| = 7$ Å; the $U_k$ from the neutron work of Ref. 100, however corrected by multiplying them by a factor of 0.728[100]; the $U_{kl}$ of the interatomic density units $\phi_\mu\phi_\nu$ from a *T L S* analysis of the experimental temperature factors.

*Figure 16* shows the latest experimental maps together with the map of the thermally smeared 4–31G + BF deformation density. *Table 8* lists the approximate deformation density maxima of all currently available density determinations.

Cyanuric acid is a particularly interesting example because it is one of the most extensively studied molecules and all available seven measured densities are derived from the same set of X-ray data[101].

The neutron parameters were determined at about 125 K[100], the X-ray data at 95 K[101]. The neutron thermal parameters were therefore adjusted to the lower temperature by multiplying them by a factor of 0.728[100]. $\Delta\varrho_{X-N/X^c}$ (cf. *Table 8*) is based on these parameters, $\Delta\varrho_{X-N/X^d}$ on a set of slightly different N/X parameters[102], $\Delta\varrho_{X-N/X^e}$ on exactly the same N/X set of thermal parameters as $\Delta\varrho_{X-N/X^c}$, and $\Delta\varrho_{X-X^e}$ on X ($1s^2$ core) parameters[103]. Amongst the M–A densities, two, $\Delta\varrho_{M-A^g}$ and $\Delta\varrho_{M-A^d}$, are of the bond-density type whereas $\Delta\varrho_{M-A^f}$ is of an interesting combined type known as two-center or population formalism. $\Delta\varrho_{M-A^f}$, $\Delta\varrho_{M-A^g}$, and $\Delta\varrho_{M-A^d}$ were calculated using the same sets of positional and thermal parameters as in the calculation of $\Delta\varrho_{X-N/X^c}$, $\Delta\varrho_{X-X^e}$, and $\Delta\varrho_{X-N/X^d}$, respectively.

X–N and X–X densities are sometimes called 'experimental' densities as they are based on measured amplitudes of structure factors whereas M–A densities are sometimes referred to as 'model' densities as the amplitudes of molecular structure factors are determined in a refinement process using appropriate atom and/or bond density units. Therefore it is correct to argue that the deviation of an M–A density from its X–N or X–X counterpart is a measure of the quality of the molecular model used if the same reference states (i.e., positional and thermal parameters) are used for both sorts of densities and if the measurements were made on a centrosymmetric crystal. Following this reasoning, only the three X–N/X and the X–X densities of *Table 8* are to be compared, one with the others. Accordingly the deviations of the

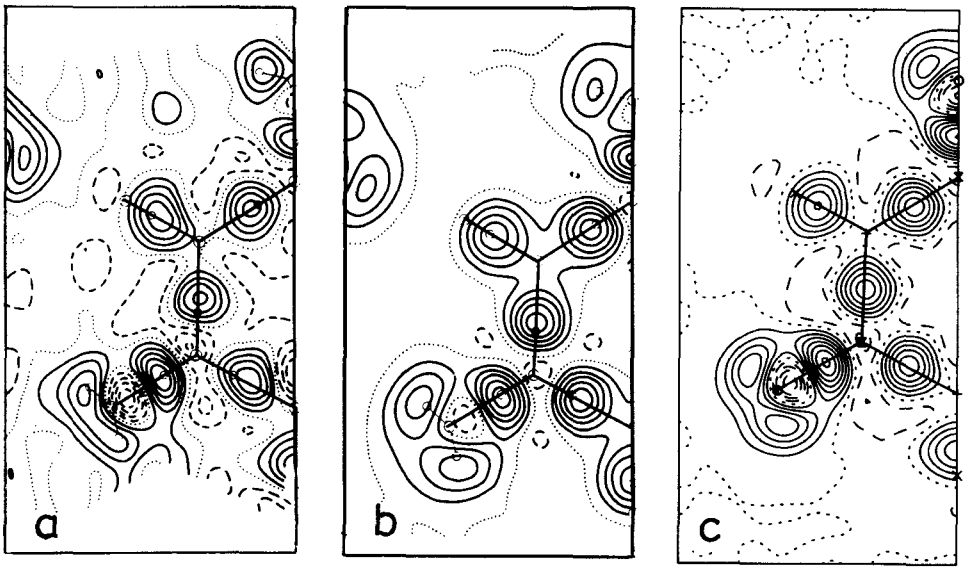


FIG. 16. Dynamic deformation density of cyanuric acid in the plane of the molecule. Positioning of atoms same as shown in the structural formula of text. Density drawn only for the left part of the molecule. (a) $\Delta\varrho_{X\text{-}N/X}(\vec{r})$ of Ref. 102 (X–N/X[d] of *Table 8*), (b) $\Delta\varrho_{M\text{-}A}(\vec{r})$ of Ref. 102 (M–A[d] of *Table 8*), and (c) $\Delta\varrho_{4\text{-}31G+BF}(\vec{r})$. Contour line interval = 0.1 e/Å$^3$. Sign convention of contour lines same as in *Figure 1*.

TABLE 8. Approximate deformation density maxima (e/Å$^3$) for cyanuric acid at 95 K

| Method | C=O[a] | C–N[a] | N–H[a] | l.p.(O)[a,b] |
|---|---|---|---|---|
| X–N/X[c] | 0.5, 0.3 | 0.5, 0.4, 0.5 | 0.5, 0.4 | 0.5, 0.3 |
| X–N/X[d] | 0.5, 0.3 | 0.4, 0.4, 0.4 | 0.4, 0.4 | 0.4, 0.3 |
| X–N/X[e] | 0.5, 0.4 | 0.5, 0.4, 0.4 | 0.5, 0.5 | 0.4, 0.3 |
| X–X[e] | 0.4, 0.3 | 0.4, 0.3, 0.4 | 0.4, 0.4 | 0.2, 0.2 |
| M–A[f] | 0.4, 0.2 | 0.5, 0.5, 0.5 | 0.5, 0.5 | 0.3, 0.2 |
| M–A[g] | 0.3, 0.3 | 0.3, 0.3, 0.3 | 0.4, 0.4 | 0.2, 0.2 |
| M–A[d] | 0.5, 0.5 | 0.5, 0.5, 0.5 | 0.4, 0.4 | 0.3, 0.3 |
| 4-31G+BF | 0.7, 0.7 | 0.5, 0.5, 0.5 | 0.4, 0.5 | 0.4, 0.4 |

[a] Various values refer to crystallographically different bonds or lone pairs.
[b] Lone pairs on oxygen.
[c] Coppens, P. and Vos, A. (1971). *Acta Cryst., B27,* 146.
[d] Dietrich, H., Scheringer, C., Meyer, H., Schulte, K.-W. and Schweig, A. (1979). *Acta Cryst., B35,* 1191.
[e] Kutoglu, A. and Scheringer, C. (1979). *Acta Cryst., A35,* 458.
[f] Jones, D. S., Pautler, D. and Coppens, P. (1972). *Acta Cryst., A28,* 635.
[g] Scheringer, C., Kutoglu, A., Hellner, E., Hase, H.-L., Schulte, K.-W. and Schweig, A. (1978). *Acta Cryst., B34,* 2162.
Scheringer, C., Kutoglu, A. and Hellner, E. (1978). *Acta Cryst., B34,* 2670.

bond maxima do not exceed ±0.1 e/Å$^3$; the deviation in the lone-pair region, however, amounts to ±0.3 e/Å$^3$.

If, however, measured deformation densities are to be compared with theoretical densities, M–A deformation densities that are based on positional and thermal parameters derived from the 'model' refinement have to be admitted as equivalent to the X–N or X–X counterparts, on the following grounds. First there is no guarantee that neutron or high-order X-ray parameters are a priori the 'best' choice for experimental reasons and secondly the 'model' parameters might be more appropriate to calculate an M–A density than are the independently measured X-ray or neutron ones. Hence, the M–A$^f$ density of *Table 8* is to be included in a comparison with the theoretical density.

In this case, the various experimental densities can deviate, one from the other, by ±0.2 e/Å$^3$. We have to attribute these deviations mostly to systematic errors in the experimental densities since the random error has frequently been estimated to be typically about ±0.05 e/Å$^3$ in the bonding regions[104].

We have shown that the deviation of 4–31G + BF densities from NHF densities is typically ±0.1 e/Å$^3$ (in the static case) in bonding and lone-pair regions. From the foregoing results, it can be expected that the correlation corrections to the types of bonds and lone pairs occurring in cyanuric acid are minor and negligible. Thus, within limits that can reasonably be expected, the agreement between experiment and theory in the C–N and N–H bonds is perfect, and in the lone-pair region satisfactory. In the C = O bond, the experimental data deviate more from the theoretical ones than they should. This deviation between experiment and theory appears to be systematic. It is also found for oxalic acid and urea (*see below*). For formamide a corresponding deviation occurs in the oxygen lone pairs.

Despite the presently unavoidable discrepancies that are dictated by systematic experimental errors of ±0.1 to ±0.3 e/Å$^3$ [27] and systematic (model) errors in the 4–31G + BF density of typically ±0.1 e/Å$^3$ in bonding and lone-pair regions, the overall agreement between the latest experimental deformation densities[102], both of the X–N or M–A types, and the 4–31G + BF density is quite impressive, as *Figure 16* demonstrates. Thus our expectations, based on the small-molecule calculations of the last section, for the particular suitability of the 4–31G + BF basis set to represent charge density distributions of large molecules are verified for cyanuric acid. We show now, with a few more examples, that 4–31G + BF and well determined experimental deformation densities are at an equal level of quality. If unusually large deviations of experimental densities from the 4–31G + BF ones occur, it is advisable to have a close look at the experimental data and evaluations.

An example is the case of tetracyanoethylene (TCNE).

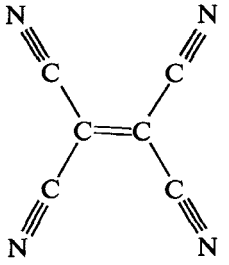

Bond lengths and angles that were used in the 4–31G + BF calculations are those given in Ref. 105 (*see Fig. 1* of this reference). The BFs used are those specified in

the text above. Thermal smearing was performed on the basis of the following data: $\sin\theta/\lambda = 0.75$ Å$^{-1}$; pseudo-unit cell dimensions: $|\vec{a}| = 8$ Å, $|\vec{b}| = 9$ Å, and $|\vec{c}| = 5$ Å; the $U_k$ from the neutron work of Ref. 106; the $U_{kl}$ from $(U_k + U_l)/2$.

*Figure 17* displays the 4-31G + BF deformation density and the latest published X–N and M–A counterparts[106]. *Table 9* summarizes the bond and lone-pair peak heights of all available density determinations.

X–N[b] (cf. *Table 9*) is based on the X-ray data of Ref. 107 and the neutron data of Ref. 105. A cubic modification was studied. A severe extinction was originally[105]

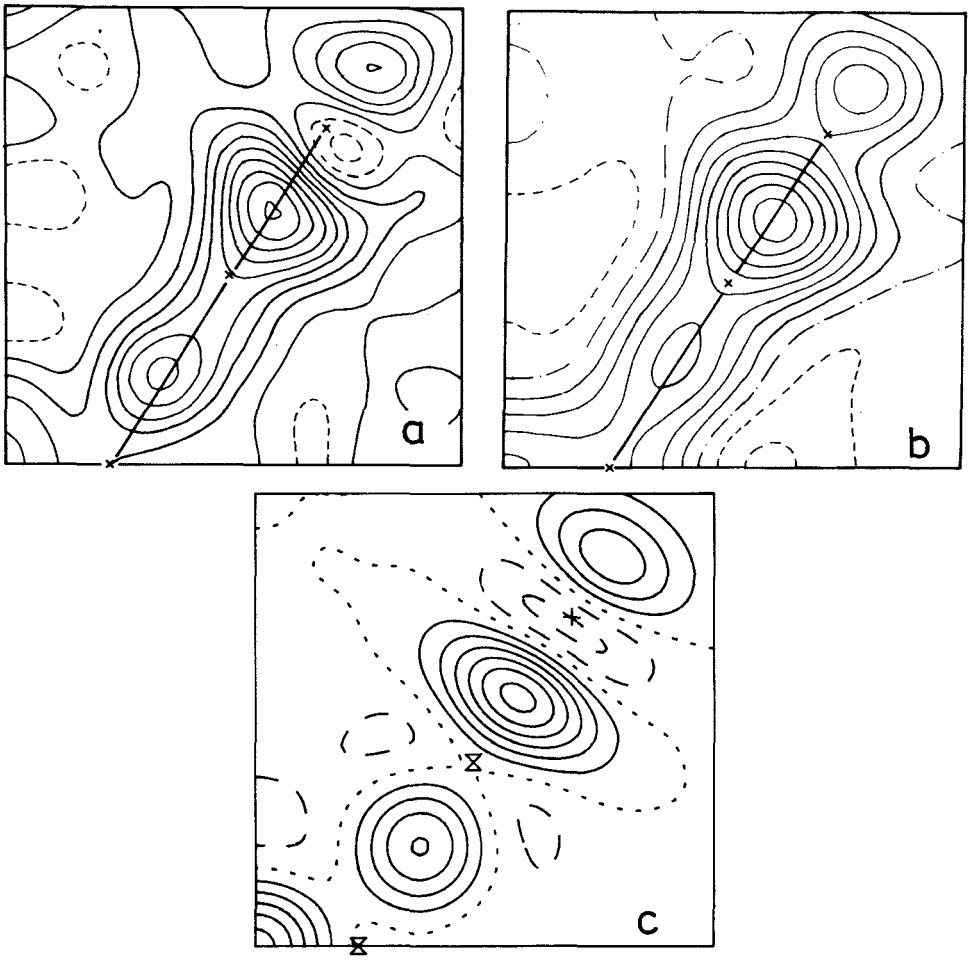


FIG. 17. Dynamic deformation density of tetracyanoethylene in the plane of the molecule. Positioning of atoms same as shown in the structural formula of text. Density drawn only for the right upper part of the molecule. (a) $\Delta\varrho_{X\text{-}N}(\vec{r})$ of Ref. 106 (X–N[c,d] of *Table 9*), (b) $\Delta\varrho_{M\text{-}A}(\vec{r})$ of Ref. 106 (M–A[c,g] of *Table 9*), and (c) $\Delta\varrho_{4\text{-}31G+BF}(\vec{r})$. Contour line interval = 0.1 e/Å$^3$. Sign convention of contour lines in $\Delta\varrho_{X\text{-}N}(\vec{r})$: zero and positive contours = full lines, negative contours = dashed lines; sign convention of contour lines in $\Delta\varrho_{M\text{-}A}(\vec{r})$: positive contours = full lines, negative contours = dashed lines, zero contour = dash-dotted line; sign convention of contour lines in $\Delta\varrho_{4\text{-}31G+BF}(\vec{r})$ same as in *Figure 1*.

TABLE 9. Approximate deformation density maxima (e/Å$^3$) for tetracyanoethylene at room temperature

| Method | C≡N | C=C | C–C | l.p.(N)[a] |
|---|---|---|---|---|
| X–N[b] | 0.9 | 0.4 | 0.6 | 0.4 |
| X–N[c,d] | 0.8 | 0.3 | 0.5 | 0.4 |
| X–N[e,f] | 0.6; 0.4[h] | 0.3 | 0.2; 0.3[h] | 0.2; 0.2[h] |
| X–X[e,f] | 0.5; 0.2[h] | 0.3 | 0.2; 0.2[h] | 0.0; 0.0[h] |
| M–A[c,g] | 0.8 | 0.4 | 0.4 | 0.4 |
| 4–31G + BF | 0.6 | 0.5 | 0.4 | 0.3 |

[a] Lone pair on nitrogen.
[b] Becker, P., Coppens, P. and Ross, F. K. (1973). *J. Am. Chem. Soc., 95,* 7604.
[c] Hansen, N. K. and Coppens, P. (1978). *Acta Cryst., A34,* 909.
[d] As in Ref. b, but an improved extinction model used.
[e] Drück, V. and Guth, H. Personal communication.
[f] Study on a monoclinic crystal, $T=295$ K, $\sin\theta/\lambda=0.90$ Å$^{-1}$, $R_i(I)=3.25\%$, $R(F_o)=3.64\%$.
[g] Multipole deformation density from refinement with positional and thermal parameters fixed at neutron values.
[h] Values for crystallographically different bonds or lone pairs.



treated with the Zachariasen formalism[108] (leading to the X–N[b] density). Applying an improved extinction model[109] leads to the X–N[c,d] density (shown in *Fig. 17*). M–A[c,g] is a multipole density based on the same X-ray data, as well as positional and thermal neutron parameters, as X–N[c,d] (M–A[c,g] is exhibited in *Figure 17*). As *Figure 17* and *Table 9* show, all three densities agree reasonably well, though X–N[c,d] is, for reasons given above, the 'best' one.

In 1977, we published a 4–31G deformation density of TCNE[26]. We tested the quality of this density by comparing the 4–31G density of $C_2N_2$ and the NHF density of Refs. 28 and 98. We concluded from the results obtained that the X–N[b] density is more in error (due to systematic errors) than the random error (±0.07 e/Å$^3$) of this determination might suggest. The results of the 4–31G + BF calculation (cf. *Table 9*) have meanwhile corroborated our previous conclusion.

These deviations between experiment and theory have stimulated some further studies. Applying an improved extinction model did not lead to marked effects[106]. Neglect of corrections for TDS (thermal diffuse scattering) in the experimental data was advocated as a likely explanation[110]. But most important, a new experimental study on a monoclinic crystal modification was undertaken[111], leading to the X–N[e,f] and X–X[e,f] density data of *Table 9*. Interestingly, the maxima in the C≡N bonds are lower in the latter densities than in the X–N[c,d] counterpart. However, the X–X[e,f] study fails in the lone-pair regions. Further studies (at 120 K on the monoclinic crystal as well as at room temperature and low temperature on the cubic crystal) are in progress[111].

The molecular geometry used for the 4–31G + BF calculations of formamide

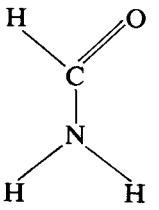

was taken from the high-order refinement of the X-ray data (*see Table 1* of Ref. 113) and the BF exponents from *Table 6*. Approximate vibrational averaging of the static density was performed with the following data: $\sin\theta/\lambda = 1.05$ Å$^{-1}$; pseudo-unit cell dimensions: $|\vec{a}| = 6.5$ Å, $|\vec{b}| = 4$ Å, $|\vec{c}| = 7$ Å; the $U_k$ from the X-ray work, refinement III, of Ref. 113; the $U_{kl}$ from $(U_k + U_l)/2$.

*Figure 18* presents a section through $\Delta\varrho_{X-X}$ and the thermally averaged $\Delta\varrho_{4\text{-}31G+BF}$. *Table 10* lists the approximate bond and lone-pair deformation density maxima.

The agreement between the X–X[112,113] and 4–31G + BF results is very good in all bonding regions. However, there is considerably less density in the experimental than in the calculated lone-pair regions, the largest difference being 0.2 e/Å$^3$. Interestingly, the AHF[c] density of Ref. 16 that is based on a C, N, O [4s3p1d] H [4s1p] CGTO set and the thermal smearing procedure of Ref. 114 is very similar to the 4–31G + BF density and is thus also appreciably higher in the lone-pair regions than its experimental counterpart. The satisfactory agreement between the two independent calculations does not correspond to a basis set error or an error due to inadequacies in the thermal averaging procedures. In view of the abovementioned experience with the magnitude of correlation densities, as well as our experience with the magnitude of effects on deformation densities due to crystal effects (*see below*), correlation and intermolecular effects (e.g., hydrogen bonding) of this order of magnitude are precluded. We have to presume therefore that the X–X density is in error in the formamide lone-pair region.

In order to facilitate comparisons with recently published AHF densities[115,116], the geometrical parameters from the neutron diffraction study of $\alpha$-deuterooxalic acid[117] were chosen for our 4–31G + BF calculations of oxalic acid.

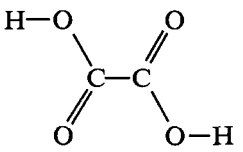

The BF exponents were taken from *Table 6*. The following data were used in the thermal averaging procedure: $\sin\theta/\lambda = 1.2$ Å$^{-1}$; pseudo-unit cell dimensions: $|\vec{a}| = 11$ Å, $|\vec{b}| = 6$ Å, $|\vec{c}| = 4$ Å; the $U_k$ from the X-ray work, refinement II, of Ref. 118; the $U_{kl}$ from a *T L S* analysis.

*Figure 19* displays the X–X–, the M–A–, and the dynamic 4–31G + BF deformation densities in the plane of the oxalic acid molecule. *Table 11* lists the approximate maxima in all available dynamic densities.

At first, the agreement between the two thermally averaged theoretical densities (AHF[e] and 4–31G + BF) is satisfactory (discrepancies not higher than ±0.1 e/Å$^3$), as is evident from *Table 11*. For the AHF[e] density[116] a C,O [4s3p1d] H [4s1p] CGTO basis set was used. The agreement between the M–A and the 4–31G + BF (cf. *Figure 19* and *Table 11*) is good, with the exception of the C=O and OH oxygen lone-pair regions which are clearly underrated in the experimental density. Obviously, also the X–X density underrates the peak height of the OH oxygen lone pair as compared to the theoretical densities (by 0.2 or 0.3 e/Å$^3$). The X–X peak heights of the C=O, C–O, and O–H bonds, as well as of one of the C=O oxygen lone pairs, are slightly lower than the corresponding peaks in the M–A and theoretical densities (largest discrepancy, 0.2 e/Å$^3$, in the C=O bond).

*Table 12* summarizes the peak heights in the static deformation densities of oxalic acid that are currently available. The basis set chosen for the AHF[d] calculation of

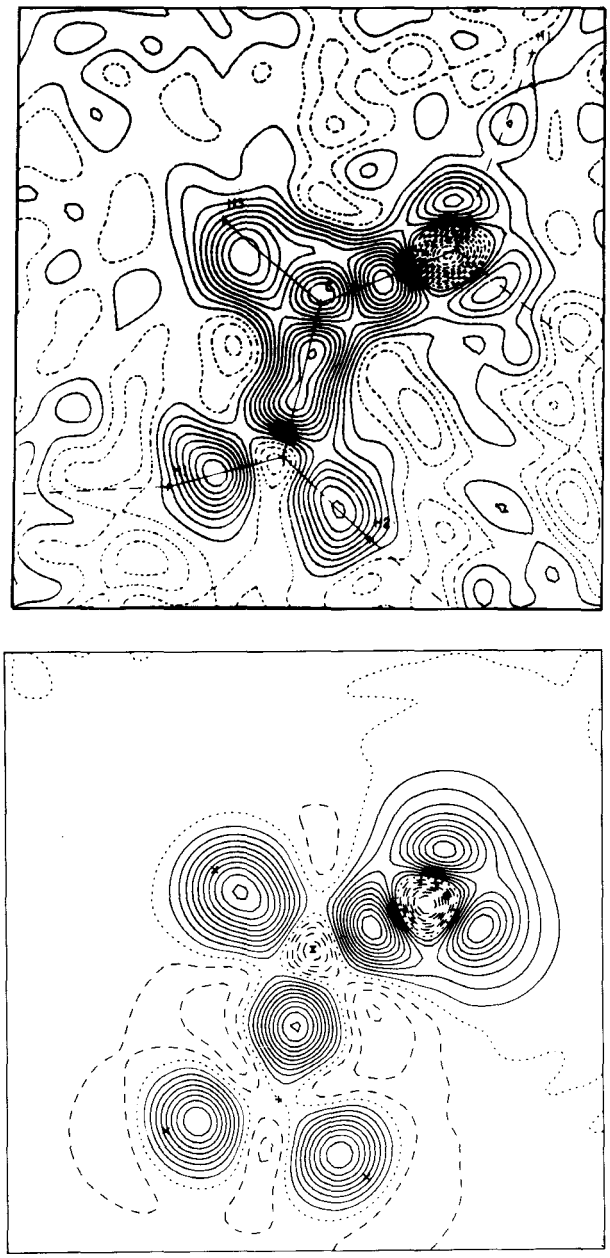


FIG. 18. Dynamic deformation density of formamide in the plane of the molecule. Positioning of atoms same as shown in the structural formula of text. (a) $\Delta\varrho_{X-X}(\vec{r})$ of Refs. 112 and 113 ($X-X^{b,c}$ of *Table 10*) and (b) $\Delta\varrho_{4\text{-}31G+BF}(\vec{r})$. Contour line interval = 0.05 e/Å$^3$. Sign convention of contour lines in $\Delta\varrho_{X-X}(\vec{r})$: zero and positive contours = full lines, negative contours = dashed lines; sign convention of contour lines in $\Delta\varrho_{4\text{-}31G+BF}(\vec{r})$ same as in *Figure 1*.

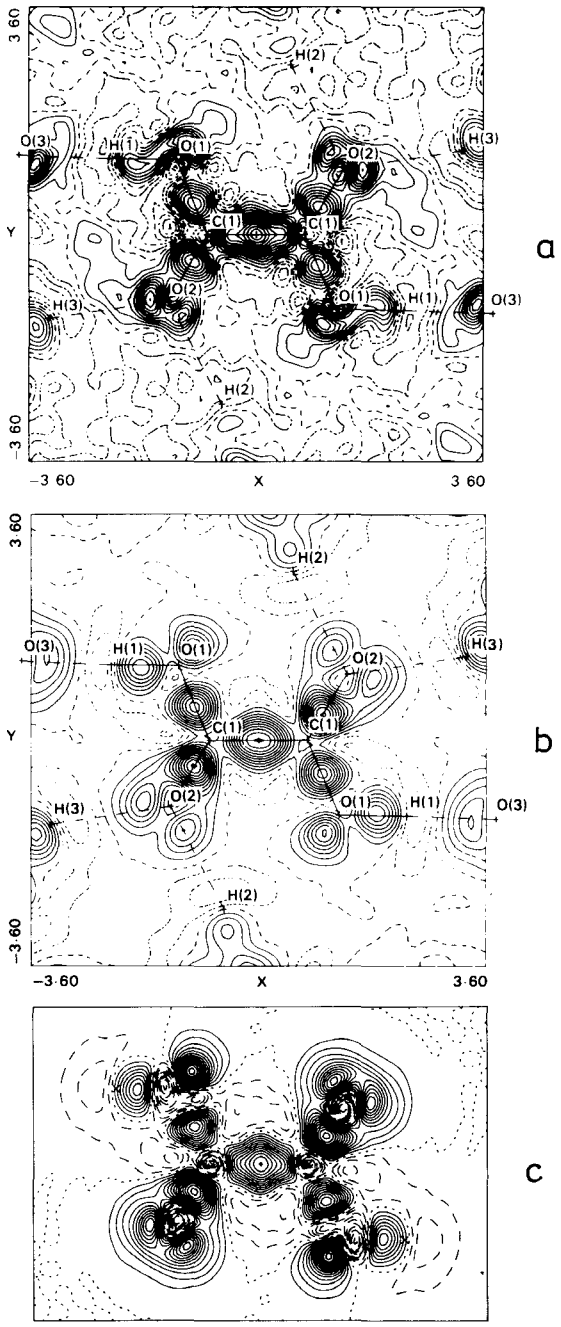


FIG. 19. Dynamic deformation density of oxalic acid in the plane of the molecule. Positioning of atoms same as shown in the structural formula of text. (a) $\Delta\varrho_{X-X}(\vec{r})$ of Ref. 118 (X–X$^{c,d}$ of *Table 11*), (b) $\Delta\varrho_{M-A}(\vec{r})$ of Ref. 118 (M–A$^{c,d}$ of *Table 11*), and (c) $\Delta\varrho_{4-31G+BF}(\vec{r})$. Contour line interval = 0.05 e/Å$^3$. Sign convention of contour lines in $\Delta\varrho_{X-X}(\vec{r})$ and $\Delta\varrho_{M-A}(\vec{r})$: positive contours = full lines, negative contours = dotted lines, zero contour = dashed line; sign convention of contour lines in $\Delta\varrho_{4-31G+BF}(\vec{r})$ same as in *Figure 1*.

TABLE 10. Approximate deformation density maxima (e/Å$^3$) for formamide at 90 K

| Method | C=O | C–N | C–H | N–H | l.p.(O)[a] |
|---|---|---|---|---|---|
| X–X[b,c] | 0.50 | 0.50 | 0.40 | 0.35, 0.35 | 0.30, 0.20 |
| AHF[c] | 0.40 | 0.45 | 0.60 | 0.40, 0.40 | 0.40, 0.40 |
| 4–31G + BF | 0.50 | 0.50 | 0.50 | 0.40, 0.40 | 0.45, 0.40 |

[a] Lone pairs on oxygen.
[b] Stevens, E. D. (1978). *Acta Cryst., B34,* 544.
[c] Stevens, E. D., Rys, J. and Coppens, P. (1978). *J. Am. Chem. Soc., 100,* 2324.

TABLE 11. Approximate deformation density maxima (e/Å$^3$) for oxalic acid at 100 K

| Method | C–C | C=O | C–O | O–H | l.p.(C=O)[a] | l.p.(OH)[b] |
|---|---|---|---|---|---|---|
| X–X[c,d] | 0.65 | 0.50 | 0.35 | 0.25 | 0.50; 0.35 | 0.40 |
| M–A[c,d] | 0.50 | 0.60 | 0.45 | 0.30 | 0.25; 0.20 | 0.35 |
| AHF[e] | 0.55 | 0.60 | 0.40 | 0.35 | 0.50; 0.50 | 0.60 |
| 4–31G + BF | 0.60 | 0.70 | 0.50 | 0.35 | 0.55; 0.50 | 0.70 |

[a] Lone pairs on carbonyl oxygen.
[b] Lone pair on hydroxyl oxygen.
[c] Stevens, E. D. and Coppens, P. (1980). *Acta Cryst., B36,* 1864.
[d] M–A IAM reference state differs from the corresponding X–X state.
[e] Stevens, E. D. (1980). *Acta Cryst., B36,* 1876.



Ref. 116 was specified above. For the AHF[c] density of Ref. 115, a C,O [5s3p1d] H [3s1p] CGTO basis set was used. Although the basis sets of the two AHF calculations contain only one set of d functions for a heavy atom (and are thus clearly not of NHF quality), the number of AFs involved is 132 (AHF[c]) or 128 (AHF[d]) compared to only 80 in the economical 4–31G + BF case. Nonetheless, the results of all three calculations (cf. *Table 12*) are similar.

The 4–31G + BF calculations of urea

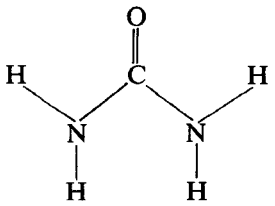


are based on the positional parameters for the so-called 'best' deformation density (*see Table 2* of Ref. 119) and the BF exponents as specified above. For thermal smearing of the static density, the following data are used: $\sin\theta/\lambda = 0.9$ Å$^{-1}$; pseudo-unit cell dimensions: $|\vec{a}| = 8$ Å, $|\vec{b}| = 4$ Å, and $|\vec{c}| = 7.5$ Å; the $U_k$ parameters according to the so-called 'best' deformation density (*see Table 2* of Ref. 119); the $U_{kl}$ from the $T$ and $L$ tensors given in Ref. 119.

*Figure 20* shows a cross-section through the 'best' experimental[119] and vibrationally averaged 4–31G + BF deformation densities. *Table 13* presents the approximate peak heights in the various available deformation densities.

A look at the data of *Table 13* reveals that much work has been devoted to deriving a 'best' experimental deformation density for urea that is based on the

TABLE 12. Approximate peak heights (e/Å$^3$) in the static deformation density of oxalic acid

| Method | C–C | C=O | C–O | O–H | l.p.(C=O)[a] | l.p.(OH)[b] |
|---|---|---|---|---|---|---|
| AHF[c] | 0.75 | 0.70 | 0.55 | 0.55 | 1.25 | 1.05 |
| AHF[d] | 0.65 | 0.70 | 0.50 | 0.55 | 1.20 | 1.10 |
| 4-31G+BF | 0.65 | 0.85 | 0.70 | 0.60 | 1.15 | 1.10 |

[a] Lone pairs on carbonyl oxygen.
[b] Lone pair on hydroxyl oxygen.
[c] Johansen, H. (1979). *Acta Cryst., A35,* 319.
[d] Stevens, E. D. (1980). *Acta Cryst., B36,* 1876.

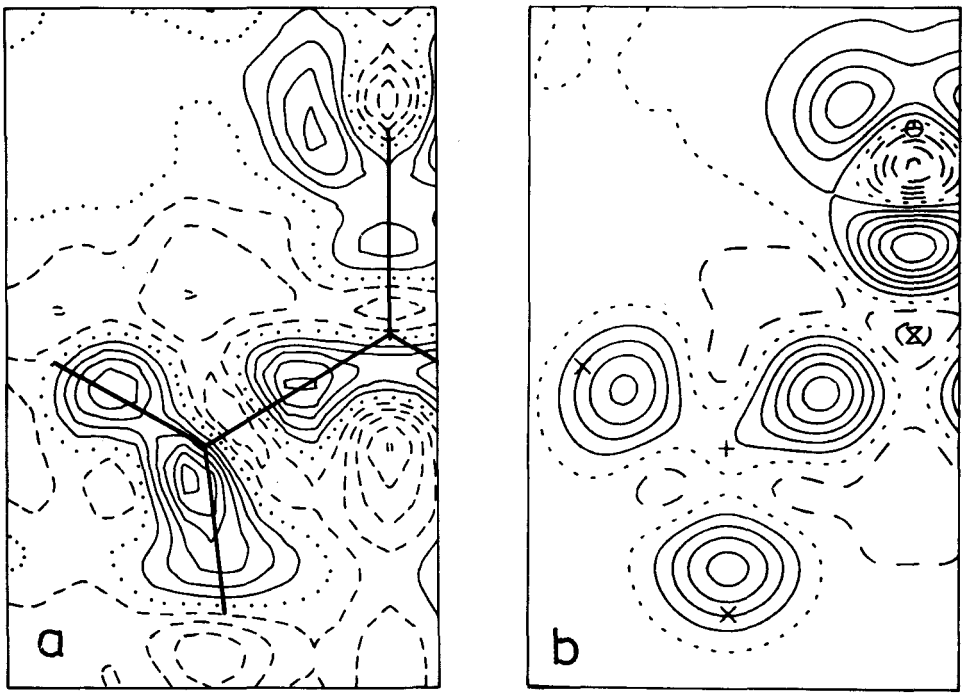


FIG. 20. Dynamic deformation density of urea in the plane of the molecule. Positioning of atoms same as shown in the structural formula of text. Density drawn for slightly more than the left part of the molecule. (a) $\Delta\varrho_{X\text{-}N/X}(\vec{r})$ of Ref. 119 ($X\text{-}N/X^{f,g,j}$ of *Table 13*) and (b) $\Delta\varrho_{4\text{-}31G+BF}(\vec{r})$. Contour line interval = 0.1 e/Å$^3$. Sign convention of contour lines same as in *Figure 1.*

X-ray data of Ref. 120 and the neutron data of Ref. 119. Despite these efforts, the final result (*see Fig. 20 and Table 13*) is still not in satisfactory agreement with the corresponding theoretical outcome. The deviation of the 'best' experimental density (i.e., the $X\text{-}N/X^{f,g,j}$ density of *Table 13*) is particularly striking in the C=O bonding region, where the 'best' experimental result underrates the density by about 0.4 e/Å$^3$.

TABLE 13. Approximate deformation density maxima (e/Å$^3$) for urea at 100 K[a,b]

| Method | C=O | C–N | N–H[c] | l.p.(O)[d] |
|---|---|---|---|---|
| M–A[e] | 0.1 | 0.2 | 0.4; 0.3 | 0.4 |
| X–N/X[f,g,h] | 0.1 | 0.3 | 0.3; 0.3 | 0.9 |
| X–X[f,g,i] | 0.2 | 0.5 | 0.6; 0.6 | 0.3 |
| X–N/X[f,g,j] | 0.2 | 0.5 | 0.4; 0.6 | 0.4 |
| 4–31G+BF | 0.6 | 0.5 | 0.4; 0.4 | 0.4 |

[a] Temperature originally specified as 123 K: Ref. b; later corrected to about 100 K: Ref. f.
[b] Mullen, D. and Hellner, E. (1978). *Acta Cryst., B34,* 1624.
[c] Various values refer to crystallographically different bonds.
[d] Lone-pair region on oxygen.
[e] Scheringer, C., Mullen, D., Hellner, E., Hase, H.-L., Schulte, K.-W. and Schweig, A. (1978). *Acta Cryst., B34,* 2241.
[f] Guth, H., Heger, G., Klein, S., Treutmann, W. and Scheringer, C. (1980). *Z. Kristallogr., 153,* 237.
[g] Phases and scale factor from the M–A model.
[h] Neutron thermal parameters at 123 K adjusted to the X-ray data.
[i] Atomic parameters used are the 1 s$^2$ parameters from Ref. b.
[j] So-called 'best' deformation density based on the phases and scale factor of Ref. g and a mixture of neutron and X-ray (1 s$^2$) atomic parameters.



The X-ray data were collected at a temperature specified as 123 K[120]. A later neutron diffraction study at 60, 123 and 293 K[119] revealed that the temperature of the X-ray investigation was probably about 100 K. The neutron data had therefore to be adjusted to the X-ray data using the method of Ref. 100. Moreover, since the urea crystal is non-centrosymmetric, the X–N/X[f,g,h], X–X[f,g,i] and X–N/X[f,g,j] deformation densities were based on the phases and scale factor of the molecular refinement of Ref. 121. The basic model of this refinement is of the bond-density type, and was also used to calculate the M–A density of *Table 13.*

It must be stressed again that there is no indication at all, at present, that the differences between the $\Delta\varrho_{X-N/X}$ and $\Delta\varrho_{4-31G+BF}$ densities that are evident from *Figure 20* (mainly in the C=O bond, but also in the N–H bonding regions) could be ascribed to crystal effects. It is obviously useful for the experimentalists to have a reliable theoretical density at hand.

The positional parameters for the 4–31G + BF calculation of thiourea

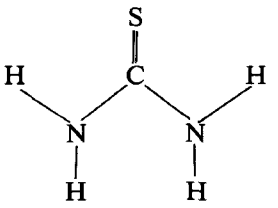


were taken from the neutron diffraction investigation of Ref. 122. The exponents of the BFs are those specified above. Thermal smearing was carried out with the following data: $\sin\theta/\lambda = 0.9$ Å$^{-1}$; pseudo-unit cell dimensions: $|\vec{a}| = 8$ Å, $|\vec{b}| = 4$ Å,

and $|\vec{c}| = 7.5$ Å; the $U_k$ from the neutron work of Ref. 122 and the $U_{kl}$ from a *T L S* analysis of these data.

*Figure 21* shows the X–X and M–A deformation densities of molecule 1 in the asymmetric unit as well as the dynamic 4–31G + BF deformation density[123]. *Table 14* lists the corresponding approximate deformation density maxima for molecule 1 and additionally molecule 2 in the asymmetric unit.

As the maps of *Figure 21* and the data of *Table 14* show, the agreement between the experimental densities for molecule 1 and the theoretical density is satisfactory (deviations in bond and lone-pair peak heights are less than ±0.1 e/Å$^3$). The

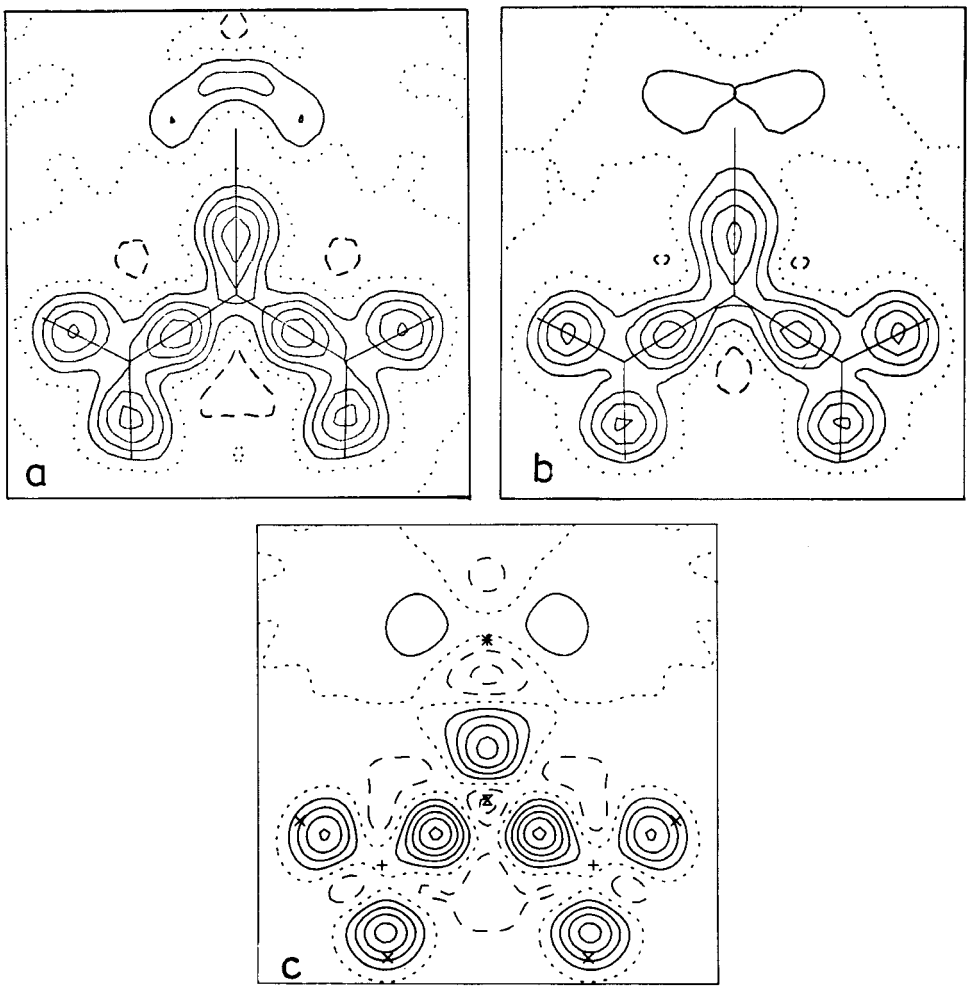


FIG. 21. Dynamic deformation density of thiourea in the plane of the molecule. Positioning of atoms same as shown in the structural formula of text. Experimental densities refer to molecule 1 in the asymmetric unit. (a) $\Delta\varrho_{X-X}(\vec{r})$ of Ref. 123 (X–X$^{d,e}$ of *Table 14*), (b) $\Delta\varrho_{M-A}(\vec{r})$ of Ref. 123 (M–A$^{d,f}$ of *Table 14*), and (c) $\Delta\varrho_{4-31G+BF}(\vec{r})$. Contour line interval = 0.1 e/Å$^3$. Sign convention of contour lines same as in *Figure 1*.

TABLE 14. Approximate deformation density maxima (e/Å$^3$) for thiourea at 123 K

| Method | C=S[a] | C–N[a] | N–H[a,b] | l.p.(S)[a,c] |
|---|---|---|---|---|
| X–X[d,e] | 0.1; 0.4 | 0.4; 0.4 | 0.4, 0.4; 0.4, 0.4 | 0.2; 0.2 |
| M–A[d,f] | 0.1; 0.4 | 0.4; 0.4 | 0.4, 0.4; 0.4, 0.4 | 0.1; 0.1 |
| 4–31G+BF[d] | 0.4 | 0.5 | 0.4, 0.4; 0.4, 0.4 | 0.1; 0.1 |

[a] Values right or left of semicolon refer to molecule 1 or 2 in the asymmetric unit.
[b] Values right or left of comma refer to crystallographically different bonds.
[c] Lone-pair region on sulfur.
[d] Kutoglu, A., Scheringer, C., Meyer, H. and Schweig, A. (1982). *Acta Cryst., B38,* 2626.
[e] Phases from the molecular model (*see* M–A).
[f] Reference state different from the X–X reference state.

agreement for molecule 2 is equally satisfactory in the C–N, N–H, and lone-pair regions. However in the C=S bond, the experimental density is too low by 0.3 e/Å$^3$.

In order to exclude hydrogen bonding as responsible for such an effect, we carried out a 4–31G+BF model calculation on the system $H_2C=S\cdot 3HF$ with the positions of C and S in $H_2CS$ and of the three H atoms in the HF molecules the same as in the thiourea crystal. As a result, no change in the height of the C=S peak (nor of any other peak) occurred, even in the static density.

The material presented above demonstrates that the agreement between the 'best' experimental deformation densities and the 4–31G+BF densities is very close. In particular, where more than one experimental density has been determined, the 'best' of these densities which is, as a rule, the most recent one, is the closest to the 4–31G+BF density. *It can be stated, therefore, that the 4–31G+BF deformation density sets a helpful standard to experimentalists in their often quite complicated search for the 'best' experimental result.* If larger deviations from the 4–31G+BF deformation density occur, a reconsideration of the experimental data and models appears to be opportune.

### *3.4 Hydrogen-bonding effects on deformation densities in molecular crystals*

Strict comparisons between experimental deformation densities of hydrogen-bonded molecular crystals and theoretical deformation densities of hydrogen-bonded molecular complexes have not previously been made. All published theoretical densities[115,116,124–129] of hydrogen-bonded complexes are static densities and, with the exception of the densities of Refs. 115 and 116, are difference densities between the density of the complex and the sum of the densities of the constituent molecules, instead of the usual deformation densities. A review article on the influence of hydrogen bonding on charge densities is available[130].

Below we present the first comparison between experimental (crystal) deformation densities and theoretical densities of suitably chosen molecular complexes taking hydrogen peroxide and $\alpha$-oxalic acid dihydrate as representative examples for weak and strong hydrogen bonding, respectively.

In a hydrogen peroxide crystal, each end of the $H_2O_2$ molecule donates one and accepts another hydrogen bond from a neighbouring molecule[44]. All O · · · H bonds are identical. Therefore, entities of either five $H_2O_2$ molecules or eight $H_2O_2$ molecules should be chosen for the calculation of the effects of hydrogen bonding on one particular $H_2O_2$ molecule or one particular O · · · H–O bonding region, respectively. $[(H_2O_2)_8]$ is beyond our computer facilities. Furthermore, hydrogen

bonding is expected to be weak in the present example (O · · · H bond length at 110 K = 1.98 Å from an X-ray determination and = 1.786 Å from neutron work[44]). Therefore we restrict ourselves to the simplest model case, namely $[(H_2O_2)_2]$.

The 4–31G + BF calculations of the static and dynamic densities of $[(H_2O_2)_2]$ are based on the same data as described above for $H_2O_2$ except for the somewhat enlarged pseudo-unit cell dimensions: $|\vec{a}| = 7.5$ Å, $|\vec{b}| = 6$ Å, and $|\vec{c}| = 9$ Å. The intermolecular $U_{kl}$ were derived in the same way as the intramolecular ones. One s BF with an orbital exponent of 0.3 was placed at the midpoint of the O · · · H bond. The orbital exponent was optimized for $[(H_2O)_2]$ with the O · · · H distance being fixed to the value found for the $H_2O_2$ crystal.

Notably, the deformation densities of the molecular complexes considered in the present work (i.e., $[(H_2O_2)_2]$ as well as $[(COOH)_2 \cdot 2H_2O]$) stay practically unaltered when the O · · · H bond function is omitted.

*Figure 22* exhibits a section of the X–N and the dynamic $[(H_2O_2)_2]$ densities through the atoms O · · · H–O involved in the hydrogen bond. *Table 15* lists the approximate deformation density maxima in the plane.

Both *Figure 22* and *Table 15* show that agreement of the experimental and theoretical model densities is satisfactory in the O–H bond, in the lone-pair region of the donor molecule and in one of the lone-pair regions of the acceptor molecule, but that there is marked disagreement in the other lone-pair region of the acceptor molecule.

The confrontation of *Figures 22a and b* shows that the distinct asymmetry of the lone-pair regions on the oxygen atom of the acceptor molecule cannot be traced back to the formation of the O(acceptor) · · · H–O(donor) bond. This asymmetry has been mentioned in a preceding section.

The difference between the dynamic deformation densities of the $[(H_2O_2)_2]$ complex and the density built up from the superimposed densities of two $H_2O_2$ molecules is negligible in all relevant regions. The results show that hydrogen bonding between two $H_2O_2$ molecules does not lead to any marked effects in the deformation density.

In $\alpha$-oxalic acid[131] each O–H group donates a hydrogen bond to a water molecule and each C = O group accepts two hydrogen bonds from two water molecules. Each water molecule is a proton donor in two bonds to oxalic acid molecules and a proton acceptor in a third bond to an oxalic acid molecule. Amongst the many O · · · H bonds in such a large hydrogen-bonded aggregate (i.e., a particular oxalic acid molecule surrounded by six water molecules with each being bonded to another two oxalic acid molecules), two are distinguished from all others by a rather short bond length of about 1.4 Å (bond lengths of all other hydrogen bonds about 1.9–2.0 Å). Therefore a hydrogen-bonded complex $[(COOH)_2 \cdot 2H_2O]$ consisting of one oxalic acid molecule and the two water molecules that accept the short (strong) hydrogen bonds

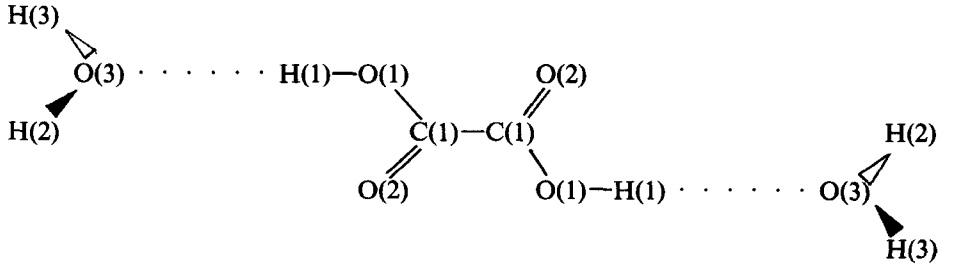

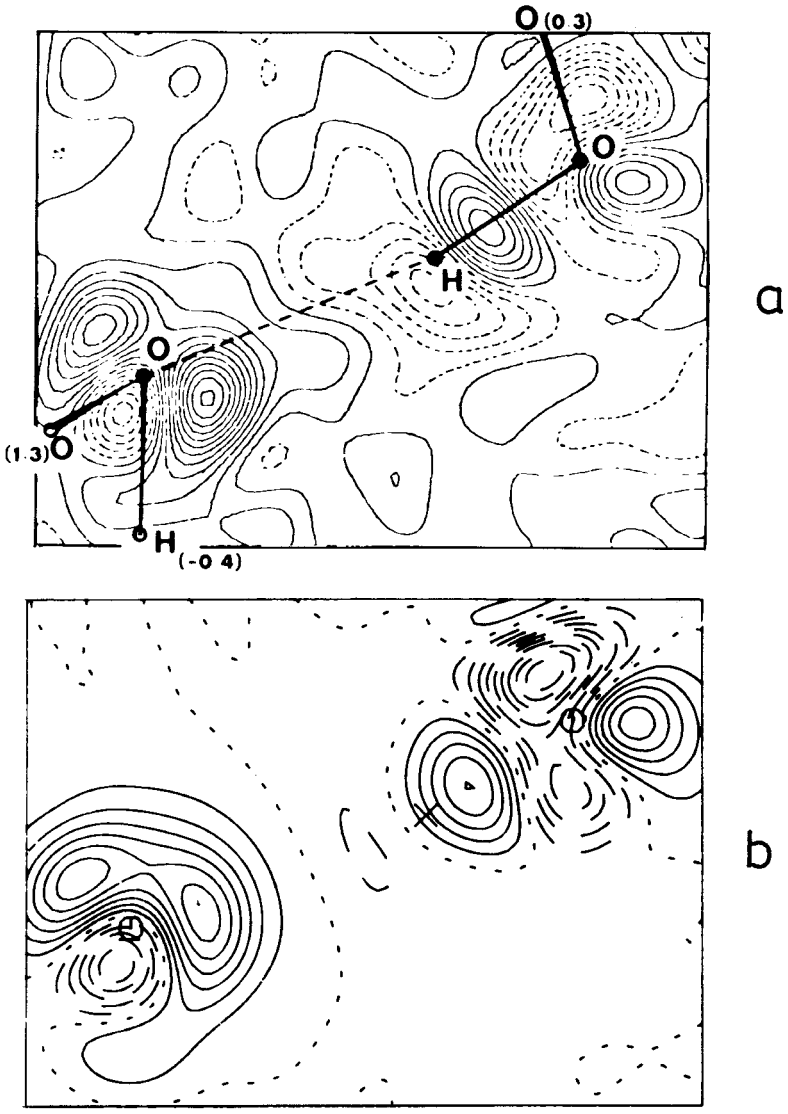


FIG. 22. Section of the dynamic deformation density of hydrogen peroxide through the atoms O · · · H–O involved in the hydrogen bond. (a) $\Delta\varrho_{X-N}(\vec{r})$ of Ref. 44 (X-N[d] of *Table 5*) and (b) $\Delta\varrho_{4-31G+BF}(\vec{r})$. Contour line interval = 0.1 e/Å$^3$. Sign convention of contour lines same as in *Figure 6*.

appears to be a reasonable model for investigating the effects of this bond on the deformation density of oxalic acid.

The 4–31G + BF calculation of the static density of the complex is based on the positional parameters of Ref. 117 and the BF exponents of Table 6. Additionally, one s BF with an exponent of 0.5 was placed in each O · · · H bond. The orbital exponent was optimized for $[(H_2O)_2]$ with the O · · · H distance kept fixed to the value determined for the strong O · · · H bonds in the $\alpha$-oxalic acid dihydrate

TABLE 15. Approximate deformation density maxima (e/Å$^3$) for hydrogen peroxide at 110 K in a section through the atoms O . . . H–O involved in the hydrogen bond

| Method | O–H[a] | l.p.(O)[a] | l.p.(O)[b,c] | l.p.(O)[b,d] |
|---|---|---|---|---|
| X–N[e] | 0.5 | 0.5 | 0.7 | 1.1 |
| 4-31G + BF/Dimer | 0.5 | 0.5 | 0.6 | 0.6 |

[a] Donor molecule.
[b] Acceptor molecule.
[c] Lone-pair region on the oxygen atom that is directed towards O (1.3), cf. *Figure 22a* of the present paper.
[d] Lone-pair region on the oxygen atom that is directed towards H (—0.4), cf. *Figure 22a* of the present paper.
[e] Savariault, J. M. and Lehmann, M. S. (1980). *J. Am. Chem. Soc., 102,* 1298.

crystal. Thermal smearing of the static density was carried out using the thermal parameters from refinement II of Ref. 118, additionally intermolecular $U_{kl}$ from $(U_k + U_l)/2$ and the pseudo-unit cell dimensions and $\sin\theta/\lambda = 1.2$ Å$^{-1}$ specified in the preceding section, for the oxalic acid molecule.

*Table 16* summarizes the approximate maxima in the X–X density[118] and in three 4–31G + BF dynamic model deformation densities, namely in the density calculated for isolated molecules of oxalic acid (discussed in detail in the preceding section) and water, in the density obtained from summing the isolated molecular densities, and in the density of the molecular complex $[(COOH)_2 \cdot 2H_2O]$. Inspection of the data clarifies two important points:

1. The strong hydrogen bonds have little influence upon the density of the oxalic acid molecule. In fact, only the 1.p.(OH)[b] maximum is reduced by 0.05 e/Å$^3$. Thus, taking into account strong hydrogen bonding does not markedly improve the discrepancies between the X–X and the 4–31G + BF (isolated molecules) data discussed in the preceding section.
2. The strong hydrogen bond has, however, a more pronounced effect on the 1.p.($H_2O$)[c] maximum. It ameliorates the agreement (by 0.1 e/Å$^3$) between experiment (X–X) and theory (isolated water molecule) in the plane of the oxalic acid molecule.

*Figure 23* exhibits the X–X[118] density and the 4–31G + BF dynamic density of the water molecule in the $[(COOH)_2 \cdot 2H_2O]$ complex and *Table 17* lists the approximate maxima in these densities. The agreement between the experimental and theoretical densities is excellent in the plane considered.

*Figure 24* shows the X–X density[132] and the 4–31G + BF deformation densities of $[(COOH)_2 \cdot 2H_2O)]$ agrees perfectly with the corresponding density of the $[(H_2O)_2]$ containing O(3) and H(1) and *Table 18* collects the approximate maxima in the densities shown in *Figure 24.* Unexpectedly, the X–X density distinctly differs from its 4–31G + BF counterpart. In particular, the lone-pair region on the oxygen atom of water exhibits only one maximum in contrast with the double maximum in the theoretical density, the peak height is markedly lower than in the theoretical density, and the shape is noticeably different from the shape of the theoretical density. There is no doubt that the theoretical map is essentially correct, since on the one hand the static lone-pair density of the water molecule of the present calculation on $[(COOH)_2 \cdot 2H_2O)]$ agrees perfectly with the corresponding density of the $[(H_2O)_2]$

TABLE 16. Approximate deformation density maxima (e/Å$^3$) for $\alpha$-oxalic acid dihydrate at 100 K in the plane of the oxalic acid molecule

| Method | C–C | C=O | C–O | O–H | l.p.(C=O)[a] | l.p.(OH)[b] | l.p.($H_2O$)[c] |
|---|---|---|---|---|---|---|---|
| X–X[d,e] | 0.65 | 0.50 | 0.35 | 0.25 | 0.50; 0.35 | 0.40 | 0.45 |
| 4-31G + BF/ isolated molecules | 0.60 | 0.70 | 0.50 | 0.35 | 0.55; 0.50 | 0.70 | 0.70 |
| 4-31G + BF/ isolated molecular densities superimposed | 0.60 | 0.70 | 0.50 | 0.35 | 0.55; 0.50 | 0.70 | 0.65 |
| 4-31G + BF/ oxalic acid dihydrate | 0.60 | 0.70 | 0.50 | 0.35 | 0.55; 0.50 | 0.65 | 0.55 |

[a] Lone pairs on carbonyl oxygen.
[b] Lone pair on hydroxyl oxygen of the oxalic acid molecule.
[c] Lone-pair region on the oxygen atom of the water molecule.
[d] Stevens, E. D. and Coppens, P. (1980). *Acta Cryst., B36,* 1864.
[e] Stevens, E. D. (1980). *Acta Cryst., B36,* 1876.



TABLE 17. Approximate deformation density maxima (e/Å$^3$) for the water molecule in $\alpha$-oxalic acid dihydrate at 100 K in the plane of the water molecule

| Method | O(3)–H(2)[a] | O(3)–H(3)[a] | l.p.(O)[b] |
|---|---|---|---|
| X–X[c] | 0.40 | 0.35 | 0.45 |
| 4-31G + BF/ oxalic acid dihydrate | 0.40 | 0.35 | 0.50 |

[a] For positioning and labeling of the respective atoms, cf. Ref. c and the structural formula shown in text.
[b] Lone-pair region on oxygen.
[c] Stevens, E. D. and Coppens, P. (1980). *Acta Cryst., B36,* 1864.

TABLE 18. Approximate deformation density maxima (e/Å$^3$) for oxalic acid dihydrate at 100 K in a section perpendicular to the plane of the water molecule and containing the O(3) . . . H(1) short hydrogen bond[a]

| Method | O–H[b] | l.p.(OH)[b,c] | l.p.($H_2O$)[d,e] |
|---|---|---|---|
| X–X[f] | 0.25 | 0.35 | 0.40 |
| 4-31G + BF/ oxalic acid dihydrate | 0.35 | 0.60 | 0.70, 0.60 |

[a] For positioning and labeling of the respective atoms, cf. Ref. e and the structural formula shown in text.
[b] Oxalic acid.
[c] Lone pair on hydroxyl oxygen.
[d] Lone-pair region on the oxygen atom of the water molecule.
[e] Values right or left of comma refer to the lone-pair regions directed away from or towards the H–O bond in oxalic acid.
[f] Stevens, E. D., Coppens, P., Feld, R. and Lehmann, M. S. (1979). *Chem. Phys. Lett., 67,* 541.

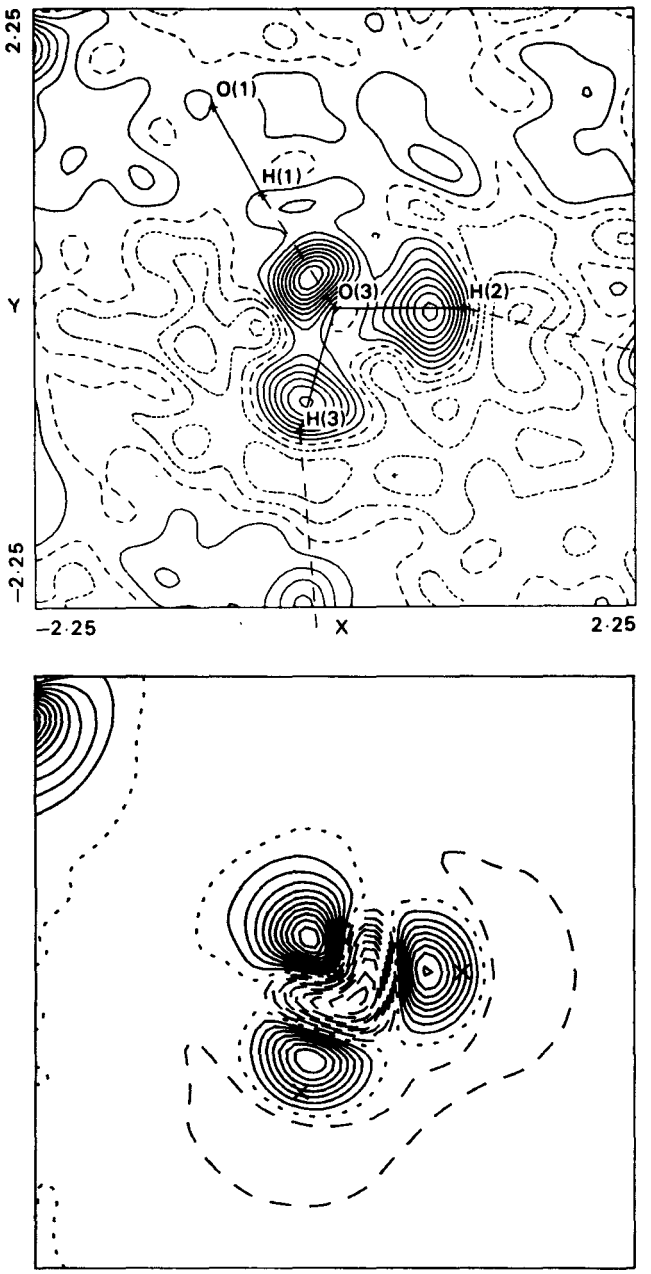


FIG. 23. Section of the dynamic deformation density of the water molecule in $\alpha$-oxalic acid dihydrate in the plane of the water molecule (for positioning and labeling of the respective atoms, cf. Ref. 118 and the structural formula shown in text). (a) $\Delta\varrho_{X-X}(\vec{r})$ of Ref. 118 (X–X$^c$ of *Table 17*) and (b) $\Delta\varrho_{4\text{-}31G+BF}(\vec{r})$ calculated for the entity oxalic acid dihydrate as depicted in the structural formula of text. Contour line interval = 0.05 e/Å$^3$. Sign convention of contour lines in $\Delta\varrho_{X-X}(\vec{r})$: positive contours = full lines, zero and negative contours = dashed lines; sign convention of contour lines in $\Delta\varrho_{4\text{-}31G+BF}(\vec{r})$ same as in *Figure 1.*

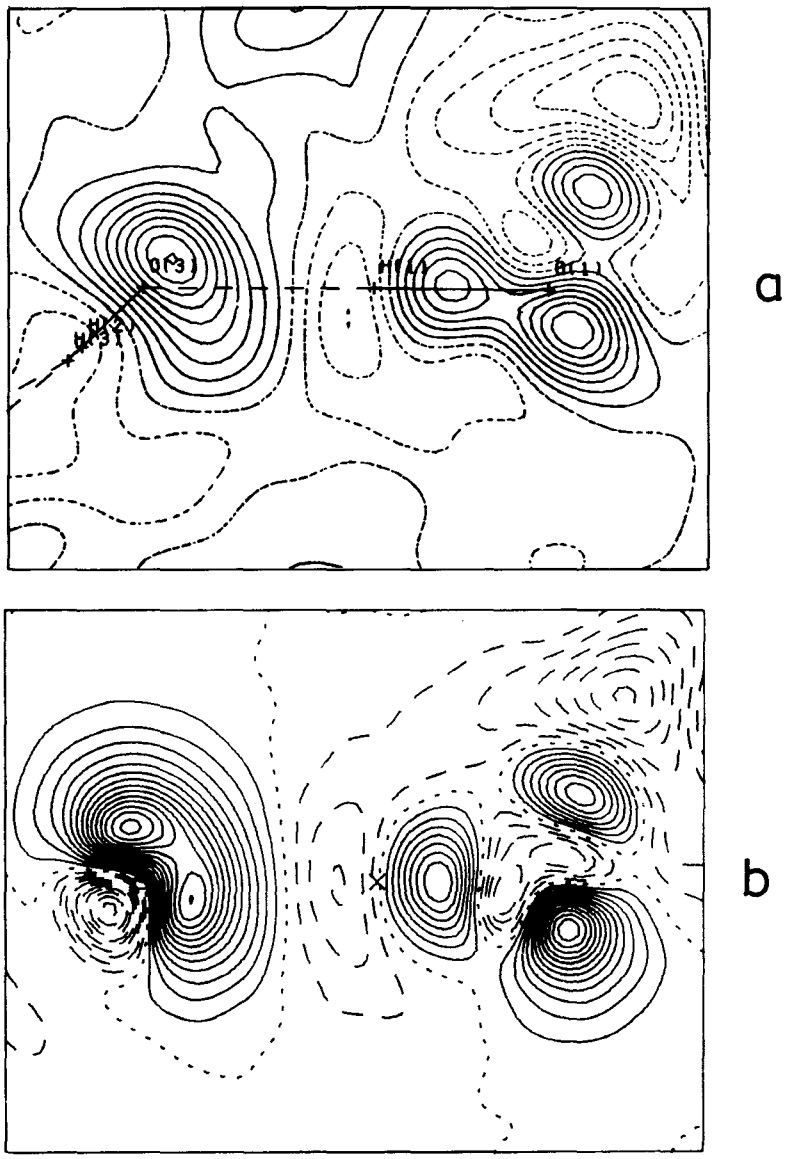


FIG. 24. Section of the dynamic deformation density of $\alpha$-oxalic acid dihydrate perpendicular to the plane of the water molecule containing O(3) and H(1) (for positioning and labeling of these atoms, cf. Ref. 118 and the structural formula shown in text). (a) $\Delta\varrho_{X-X}(\vec{r})$ of Ref. 118 ($X-X^f$ of *Table 18*) and (b) $\Delta\varrho_{4\text{-}31G+BF}(\vec{r})$. Contour line interval = 0.05 e/Å$^3$. Sign convention of contour lines in $\Delta\varrho_{X-X}(\vec{r})$ and $\Delta\varrho_{4\text{-}31G+BF}(\vec{r})$ same as in *Figure 23*.

model for [$(COOH)_2 \cdot 2H_2O$] of Ref. 116 (*Fig. 7a* of this reference), and on the other hand agreement between experiment and theory is excellent in the plane of the water molecule. Thus we have the somewhat disturbing result that the X–X density is in perfect agreement with the 4–31G + BF density in *one* plane (plane of the water molecule) but is in marked disagreement in a *second* plane (plane perpendicular to the plane of the water molecule). An explanation is urgently needed.

It had been concluded[132] that the asymmetry of the lone-pair region on the oxygen atom of water with respect to the molecular plane (of the water molecule) in the X–X density (*Fig. 24a*) indicates a polarization of its density towards the proton in the short hydrogen bond and thus is a direct indication for hydrogen bonding. Conversely, the theoretical density is polarized away from the proton of the short hydrogen bond. A detailed theoretical investigation has shown that

1. The asymmetry in the theoretical density is partly inherent in the static density built up from the superimposed molecular densities.
2. This asymmetry is enhanced by thermal smearing so that the resulting smeared superimposed density is quite close to the corresponding density in the [$(COOH)_2 \cdot 2H_2O$] complex.
3. Hydrogen bonding leads to a reduction of the peak height of the lone-pair region that is directed towards the proton by about 0.1 e/Å$^3$ and an increase in the other lone-pair maximum of about 0.05 e/Å$^3$.

We think that caution must be used when drawing conclusions from the shape of a density with respect to hydrogen bonding.

From the above results it is obvious that hydrogen bonding does not generally lead to effects on molecular deformation densities in relevant regions (bonds and lone pairs) that could easily be detected or ascribed to this type of intermolecular interaction (or crystal effect). Larger discrepancies between experimental deformation densities derived from crystals with hydrogen-bonded molecules and theoretical deformation densities calculated for isolated molecules will hardly be removed by considering hydrogen bonding in appropriate molecular complexes. In particular, caution must be used when interpreting minor changes of the shape of a deformation density as evidence for or against a hydrogen bond.

### *3.5 Crystal effects on deformation densities in salts*

Below we are concerned with the important questions:

1. How large is the effect of the charges on nearest-neighbour ions on the deformation density of one particular ion (or component in general, since also neutral components as, for example, crystal water can be present in ionic crystals) in a salt?
2. Can such an effect be seen in an experimental deformation density or, in other words, can we safely compare an experimental density (derived from measurements on an ionic crystal) with the theoretical density (calculated for an isolated ion)?

To tackle this problem, we choose a simple point-charge model[25a,25b], i.e., we represent the charged surroundings of a particular ion in a crystal by point charges on the atoms (in the case of a molecular ion obtained via a population analysis for the isolated ion) of the nearest-neighbour ion and incorporate them into the AHF

calculation of the deformation density for the ion of interest.

This simple model can easily be modified (somewhat extended) as we show with our first two cases, namely the deformation density for the formate ion in sodium formate and the azide ion in sodium azide[25a].

For the formate ion X–X, X–N, several X–N/X densities and a 4–31G+BF density of the isolated anion have been published[133]. For building up the crystal environment of the formate ion neutron data for the atomic positions[133] are used. Point charges of +1e (Na), −0.7355e (O), +0.524e (C) and −0.053e (H) are allotted to the respective atoms up to a distance of 10.0 a.u. (5.29 Å) of any atom of the selected $HCOO^-$ anion giving a total of 79 point charges. Since both oxygen atoms of $HCOO^-$ have five Na ions as closest neighbours a set of BFs is placed in each Na · · · O 'bond'. The exponents of the BFs (s 0.1, p 0.06) were determined for NaOH using the same Na · · · O distance as in NaHCOO. In order to provide the 'point-charge replacement' of the sodium ion with the capability of accepting electrons a 3s AO (taken from the (17s8p)/[4s2p] calculation of the sodium atom[134]) is additionally located at the site of the sodium ion.

The molecular geometry used for the 4–31G+BF calculation (including the crystal environment as specified above) of the formate ion

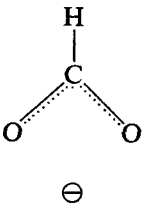


is taken from the neutron diffraction study of Ref. 133. The BF exponents are taken from *Table 6*. The data used in the thermal averaging procedure are: $\sin\theta/\lambda = 0.8$ Å$^{-1}$; pseudo-unit cell dimensions: $|\vec{a}| = 6$ Å, $|\vec{b}| = 4$ Å, $|\vec{c}| = 6$ Å; the $U_k$ from the neutron work corrected according to *Table 5* of Ref. 133; the $U_{kl}$ from $(U_k + U_l)/2$.

*Figure 25* shows a section of the X–N/X[c,f,d] (cf. *Table 19*) and the dynamic $HCOO^-$ densities without and with the crystal environment through the plane of the molecule. *Table 19* lists the approximate deformation density maxima in the respective plane.

As can be seen from *Figure 25* and *Table 19*, the effect exerted by the crystal environment is not very pronounced; the density in the C–H bond is increased by 0.1 e/Å$^3$ and the lone-pair density is decreased by 0.1 e/Å$^3$. Due to this, the agreement between the best experimental density and the theoretical density gets slightly better for the oxygen atoms but slightly worse for the C–H bond. Most important, however, the changes due to the various experimental approaches and uncertainties are of the same order of magnitude as the crystal effect (as quantified by the calculations) so that the crystal effect can hardly be extracted or proven from experiment.

Reference calculations for the two systems—isolated $HCOO^-$ with inclusion of the BFs of the Na · · · O 'bond', and $HCOO^-$ with the crystalline environment in its simplest point-charge form—have shown that the modifications mentioned above lead to minor effects only. We decided, therefore, to use the unmodified point-charge model in our treatment of the azide ion in sodium azide and, instead, pay attention to possible effects arising from making the AHF calculations self-consistent with respect to the environmental charges[25a].

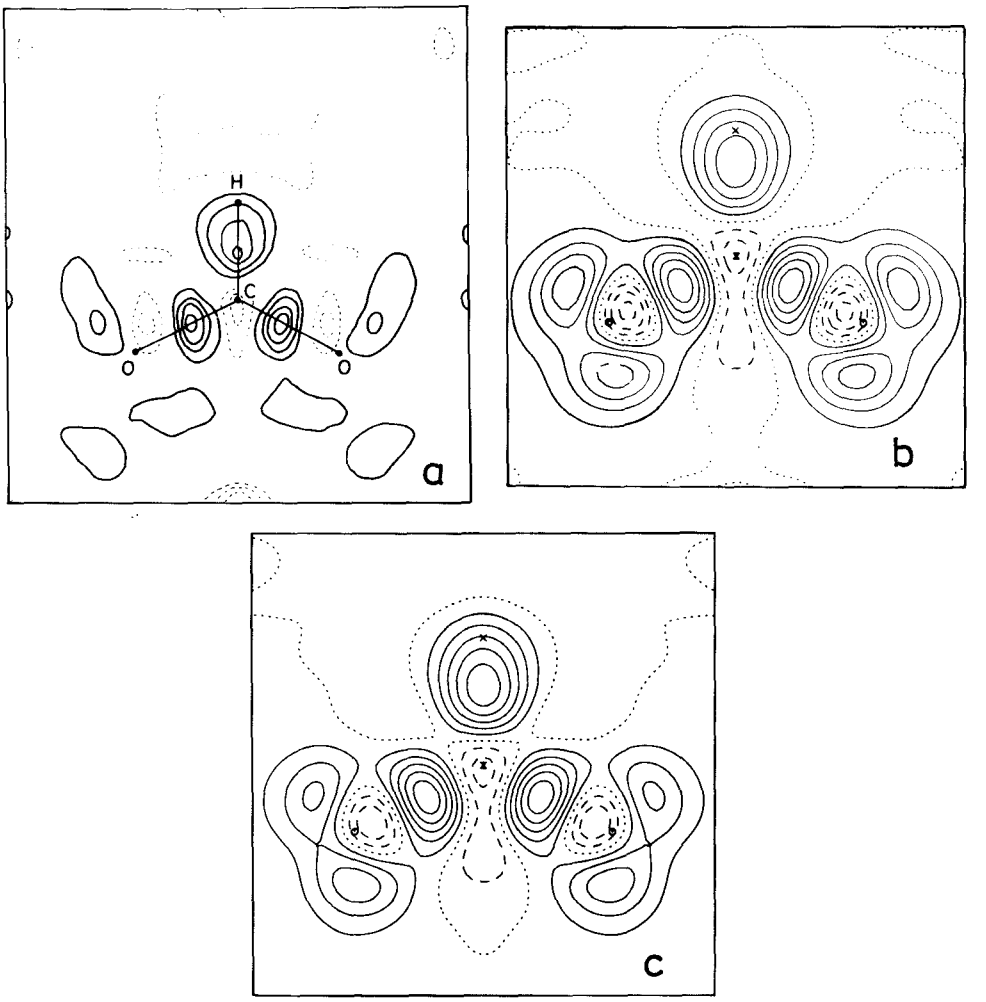


FIG. 25. Dynamic deformation density of the formate ion in sodium formate in the plane of the ion. Positioning of atoms same as shown in the structural formula of text. (a) $\Delta\varrho_{X-N/X}(\vec{r})$ of Ref. 133 ($X-N/X^{c,f,g}$ of *Table 19*), (b) $\Delta\varrho_{4-31G+BF}(\vec{r})$, and (c) $\Delta\varrho_{4-31G+BF}(\vec{r})$ under the influence of the crystal environment. Contour line interval = 0.1 e/Å$^3$. Sign convention of contour lines in $\Delta\varrho_{X-N/X}(\vec{r})$: positive contours = full lines, negative contours = dashed lines, zero contour omitted; sign convention of contour lines in both the $\Delta\varrho_{4-31G+BF}(\vec{r})$ plots same as in *Figure 1*.

TABLE 19. Approximate deformation density maxima (e/Å$^3$) for the formate ion in sodium formate at 120 K

| Method | C–O | C–H | l.p.(O)[a,b] |
|---|---|---|---|
| X–X[c,d] | 0.4 | 0.0 | 0.2, 0.1 |
| X–X[c,e] | 0.4 | 0.2 | 0.2, 0.2 |
| X–N/X[c,d,f] | 0.4 | 0.3 | 0.2, 0.1 |
| X–N/X[c,e,f] | 0.4 | 0.4 | 0.2, 0.1 |
| X–N/X[c,f,g] | 0.4 | 0.4 | 0.2, 0.1 |
| 4–31G+BF[c] | 0.5 | 0.4 | 0.4, 0.4 |
| 4–31G+BF/ crystal environment | 0.5 | 0.5 | 0.3, 0.3 |

[a] Lone pairs on oxygen.
[b] First value refers to the lone-pair lobe that is directed towards the C–H bond.
[c] Fuess, H., Bats, J. W., Dannöhl, H., Meyer, H. and Schweig, A. (1982). *Acta Cryst., B38*, 736.
[d] X-ray data set 1.
[e] X-ray data set 2.
[f] Mixture of neutron and X-ray thermal parameters.
[g] Average over data sets 1 and 2.



The 4–31G+BF calculations for the azide ion were based on the positional parameters of Ref. 135 and the BFs specified above. Taking into account all neighbouring atoms up to a distance of 14 a.u. (7.4 Å) from one of the external N atoms of $N_3^-$ a total of 168 point charges were included in the AHF calculations. The stable (self-consistent) charges on the N atoms of $N_3^-$

$$\overset{\ominus}{N} = \overset{\oplus}{N} = \overset{\ominus}{N}$$

are: −0.593e (external) and +0.186e (central). For the thermal smearing of the static density, the following data are used: $\sin\theta/\lambda = 1.2$ Å$^{-1}$; pseudo-unit cell dimensions: $|\vec{a}| = 4$ Å, $|\vec{b}| = 4$ Å, and $|\vec{c}| = 6$ Å; the $U_k$ and $U_{kl}$ are calculated from the experimentally available rigid-body thermal parameters[136].

*Figure 26* presents a cross-section through the 'best' experimental[136] (i.e., X–X[c,f], cf. *Table 20*) and the vibrationally averaged densities of the isolated ion and the ion in its chemical environment. *Table 20* collects the approximate peak heights in the various available deformation densities.

Comparison of the experimental with the theoretical results shows that the crystal effects on the deformation density of $N_3^-$ are very minor (both with respect to the bond and lone-pair maxima, i.e., less than 0.1 e/Å$^3$, and the shape of the density). In particular, the obvious differences between the shapes of the experimental and theoretical densities cannot be traced back to crystal effects. Finally, it should be added that the effects of using self-consistent charges instead of charges valid for the isolated ion are very minor.

The 4–31G+BF calculations of the thiocyanate ion (made applying the unmodified point-charge model) are performed using bond lengths and angles from the X-ray refinement of Ref. 137 and BFs as specified above. The crystal environment is mimicked by a total of 45 point charges (i.e., all charges up to 10.14 a.u.

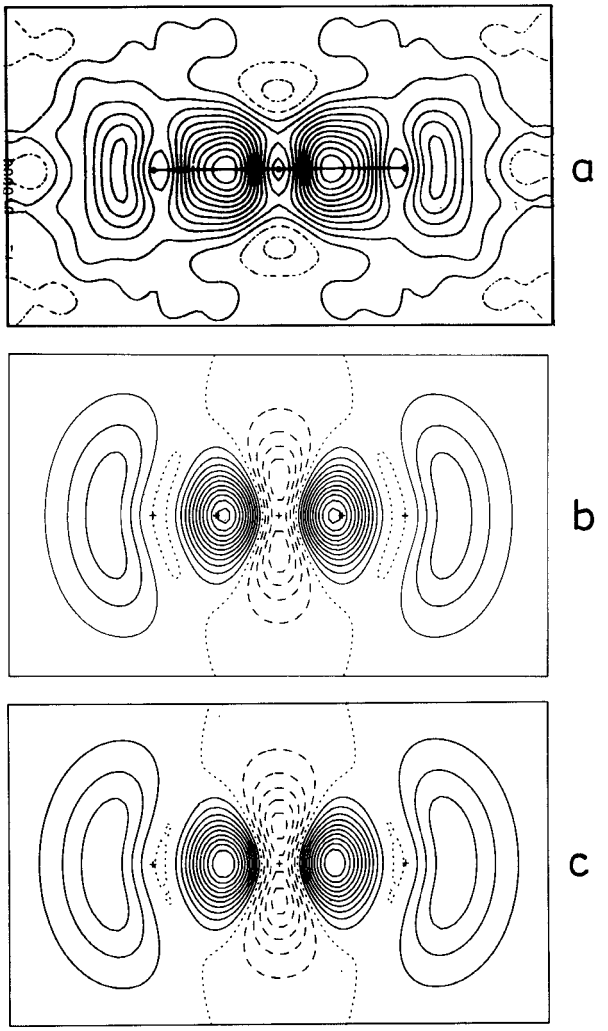


FIG. 26. Dynamic deformation density of the azide ion in sodium azide in the plane of the molecule. (a) $\Delta\varrho_{X\text{-}X}(\vec{r})$ of Ref. 136 ($X\text{-}X^{c,f}$ of *Table 20*), (b) $\Delta\varrho_{X\text{-}X}(\vec{r})$: zero and positive contours = full lines, negative contours = dashed lines; sign convention of contour lines in both the $\Delta\varrho_{4\text{-}31G+BF}(\vec{r})$ plots same as in $\Delta\varrho_{X\text{-}X}(\vec{r})$: zero and positive contours = full lines, negative contours = dashed lines; sign convention of contour lines in both the $\Delta\varrho_{4\text{-}31G+BF}(\vec{r})$ plots same as in *Figure 1.*

TABLE 20. Approximate deformation density maxima (e/Å$^3$) for the azide ion in sodium azide at room temperature[a]

| Method | N–N | l.p.(N)[b] |
|---|---|---|
| X–N[c,d] | 0.55 | 0.55 |
| X–X[c,e] | 0.50 | 0.40 |
| X–X[c,f] | 0.50 | 0.20 |
| AHF[g] | 0.40 | 0.25 |
| 4–31G + BF | 0.55 | 0.15 |
| 4–31G + BF/ crystal environment | 0.50 | 0.15 |

[a] Temperature not specified in Ref. c. The neutron work was carried out at 300 K: Choi, C. S. and Prince, E. (1976). *J. Chem. Phys., 64,* 4510. It is assumed that X-ray measurements were made at the same temperature.
[b] Lone pair on nitrogen.
[c] Stevens, E. D. and Hope, H. (1977). *Acta Cryst., A33,* 723.
[d] Using neutron parameters with second-cumulant temperature factors.
[e] Using high-order X-ray parameters with second-cumulant temperature factors.
[f] Using high-order X-ray parameters with third-cumulant temperature factors.
[g] Stevens, E. D., Rys, J. and Coppens, P. (1977). *J. Am. Chem. Soc., 99,* 265.



(5.37 Å) from the N atom and 10.13 a.u. (5.36 Å) from the S atom) of the thiocyanate anion.

$$N = C = S^{\ominus}$$

The point charges allocated to the three atoms are: −0.553e (N), +0.034e (C), and −0.481e (S). Vibrational averaging is performed at 150 K using the experimental positional and thermal parameters[137] up to the experimental limit of sin $\theta/\lambda = 0.75$ Å$^{-1}$ and the experimental unit cell ($|\vec{a}| = 5.604$ Å, $|\vec{b}| = 4.047$ Å, $|\vec{c}| = 13.279$ Å).

*Figure 27* displays a section through the experimental X–X[d,f] (cf. *Table 21*) deformation density as well as through the theoretical density of the isolated ion and the ion in the crystal. *Table 21* collects the approximate density maxima in both the experimental and theoretical deformation densities.

The 4–31G + BF/crystal environment density again differs very little (not more than approximately 0.05 e/Å$^3$) from its 4–31G + BF counterpart and the discrepancies between experiment and theory (about 0.25 e/Å$^3$) clearly exceed the crystal effect, as is obvious from *Figure 27* and *Table 21.* The discrepancies between experimental and theoretical densities thus cannot be attributed to crystal effects.

We note that a single sodium ion (and equally a single point charge replacing the sodium ion) placed at a position that is closest to the selected anion in the crystal produces much more pronounced effects on the deformation density of the anion in

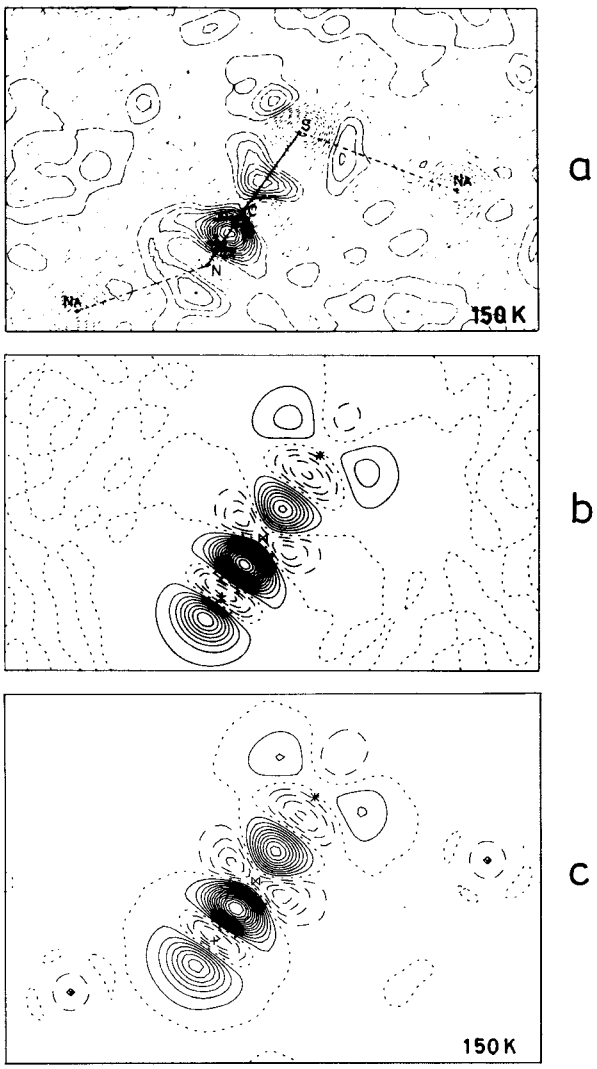


FIG. 27. Dynamic deformation density of the thiocyanate ion in sodium thiocyanate in the mirror plane. Positioning of atoms as shown in text. (a) $\Delta\varrho_{X-X}(\vec{r})$ of Ref. 137 ($X-X^{d,e}$ of *Table 21*), (b) $\Delta\varrho_{4-31G+BF}(\vec{r})$, and (c) $\Delta\varrho_{4-31G+BF}(\vec{r})$ under the influence of the crystal environment. Contour line interval = 0.05 e/Å$^3$. Sign convention of contour lines in $\Delta\varrho_{X-X}(\vec{r})$: zero and positive contours = full lines, negative contours = dashed lines; sign convention of contour lines in the $\Delta\varrho_{4-31G+BF}(\vec{r})$ maps same as in *Figure 1*.

TABLE 21. Approximate deformation density maxima (e/Å$^3$) for the thiocyanate ion in sodium thiocyanate at 150 K

| Method | C–S | C–N | l.p.(S)[a,b] | l.p.(N)[c] |
|---|---|---|---|---|
| X–X[d,e] | 0.25 | 0.60 | 0.15, 0.10 | 0.15 |
| X–X[d,f] | 0.20 | 0.45 | 0.15, 0.10 | 0.15 |
| 4–31G + BF | 0.40 | 0.75 | 0.10, 0.10 | 0.40 |
| 4–31G + BF/ crystal environment | 0.45 | 0.70 | 0.10, 0.10 | 0.35 |

[a] Lone pair region on sulfur.
[b] Second value refers to the lone-pair region that is directed towards the nearest neighbouring sodium atom.
[c] Lone pair on nitrogen.
[d] Bats, J. W., Coppens, P. and Kvick, A. (1977). *Acta Cryst., B33,* 1534.
[e] Based on the atomic parameters and scale factor from the high-order X-ray refinements.
[f] Based on the atomic parameters and scale factor from the conventional X-ray refinement.

all three cases considered[25a,138]. A more symmetrical point-charge distribution (according to the crystal structure, as described above) then leads to deformation densities (described in this section) that, in general, differ very little from the isolated ion densities.

Recently our approach of mimicking the crystalline environment of a particular ion in the deformation density calculations by directly incorporating the atomic point charges of the environment into the AHF calculation has been applied to the salts of $LiOH \cdot H_2O$[139,140] and $NaHC_2O_4 \cdot H_2O$[141]. Thermal smearing of the resulting static densities of components of these salts yields crystal effects that are again too small (compared to the accuracy of the experimental methods) to be detected[138].

To summarize, the results presented have provided answers to the questions asked above. In short, the crystalline effects in the salts studied are too small to be safely detected at present by experimental methods for determining deformation densities. Thus comparisons based on experimental densities and theoretical densities of *isolated* salt components appear to be justified.

## 4. CONCLUSION

High-quality *ab initio* calculations of electron deformation densities have been performed for small molecules. For the static near HF deformation densities (obtained with CGTO basis sets including two sets of d functions for first-row atoms) the basis set error is expected not to exceed ±0.1 e/Å$^3$ at the midpoint of a bond. The electron correlation effect on electron densities has been derived from PERTCI calculations including all singly and doubly excited configurations. The results obtained are considered to represent the (unknown) total correlation effect. The magnitude of the correlation effect turns out to be smaller than the basis set error. Thus for electron density calculations it is more important to select appropriate AHF basis sets than to include electron correlation.

For comparing theoretical and experimental deformation densities, it is important to state that we have to deal with errors of about ±0.1 e/Å$^3$ in the bonding regions of a molecule at rest and of about ±0.05 e/Å$^3$ in the same regions for a molecule moving in a crystal, in the best theoretical AHF CI deformation densities available.

These errors are generally smaller than the experimental ones (which can be as high as 0.1 to 0.3 e/Å$^3$ for a crystal). Consequently, the best calculated deformation densities have to be considered as density standards to be reached not only by less sophisticated calculations but also by experimental investigations.

For larger molecules the use of drastically reduced basis sets is unavoidable in AHF calculations. Based on small-molecule calculations the 4–31G + BF basis set has been proven to be a very suitable, economical basis set for deformation density calculations. Bond and lone-pair maxima are obtained in near HF quality, the mean deviation being less than ±0.1 e/Å$^3$. Accordingly, dynamic 4–31G + BF deformation densities compare favorably to the experimental counterparts, the theoretical results being at an equal level of quality as the most thoroughly determined experimental ones. The 4–31G + BF deformation density sets a helpful standard to experimentalists in their search for the 'best' experimental result.

The favorable comparison between the dynamic 4–31G + BF deformation density calculated for an isolated molecule and the experimental deformation density is suggested to hold even when the molecule is strongly bound in the crystal. This has been shown by investigations of hydrogen bonding and ion effects. The calculation of hydrogen-bonded aggregates of molecules leads to alterations in the bond and lone-pair regions of the dynamic deformation density of at most 0.1 e/Å$^3$ compared to isolated-molecule conditions. Similar results have been obtained for an ion with ionic surroundings simulated by a simple point-charge model. It must, therefore, be assumed that larger discrepancies between theoretical and experimental deformation densities will not be removed by considering crystal effects in the quantum-chemical calculations.

All effects considered in the density calculations of the present work (near HF basis set, electron correlation, hydrogen bonding and ion effects) are hardly detectable by comparison with experimental deformation densities at the present time. These effects will only play a major role—regarding electron deformation densities—when experimental uncertainties are diminished by nearly one order of magnitude.



## ACKNOWLEDGEMENT

This work was supported by the Deutsche Forschunsgemeinschaft, SFB 127, Projekt H2, and the Fonds der Chemischen Industrie. The quantum-chemical calculations were carried out on the TR 440 computer of the Rechenzentrum der Universität Marburg, the CDC 174 of the Rechenzentrum der Universität Gießen, the IBM 370/168 of the Rechenzentrum der Technischen Hochschule Darmstadt, and the Perkin Elmer 8/32 of the SFB 91 der Universität Kaiserslautern. The authors are indebted to Professor W. Meyer, Kaiserslautern, for making computation time available on his Perkin Elmer 8/32 computer.

## 5. REFERENCES AND FOOTNOTES

1. Part 16 of 'Comparison of observed and calculated electron densities'. Part 15: KUTOGLU, A., SCHERINGER, C., MEYER, H. and SCHWEIG, A. (1982). *Acta Cryst., B38,* 2626.
2. Parts of this work were presented by A. Schweig in lectures at the symposium on Structure analysis and theoretical chemistry, Arbeitskreis 'Kristallstrukturanalyse von Molekülverbindungen' der Fachgruppe 'Analytische Chemie' der GDCh, Darmstadt,

1980 and at the symposium on Electron distributions and the chemical bond, 181st ACS National Meeting, Atlanta, Georgia, 1981.
3. (a) University of Marburg; (b) University of Kaiserslautern.
4. BRILL, R. (1967). *Solid State Physics, 20,* 1.
5. BONHAM, R. A. (1969). *Record of Chemical Progress, 30,* 185.
6. Several articles in *Transaction of the American Crystallographic Association, Proceedings of the Symposium on Experimental and Theoretical Studies of Electron Densities,* Albuquerque, New Mexico, 1972.
7. STEWART, R. F. (1974). *Critical Evaluation of Chemical and Physical Structural Information* (eds. D. R. Lide and M. A. Paul), p. 540. Washington, D.C.: National Academy of Sciences.
8. DAWSON, B. (1975). *Advances in Structure Research by Diffraction Methods.* Oxford: Pergamon Press, and Braunschweig: Friedr. Vieweg & Sohn.
9. BADER, R. F. W. (1975). *Int. Rev. Sciences, Physical Chemistry, Series 2* (eds. A. D. Buckingham and C. A. Coulson), vol. I, p. 43. London: Butterworths.
10. COPPENS, P. (1975). *Int. Rev. Sciences, Physical Chemistry, Series 2* (ed. J. M. Robertson), vol. II, p. 21. London: Butterworths.
11. HINCHLIFFE, A. and DOBSON, J. C. (1976). *Chem. Soc. Rev., 5,* 79.
12. *Physica Scripta* (1977), *15,* 66–157.
13. *Isr. J. Chem.* (1977), *16,* 87–229.
14. COPPENS, P. and STEVENS, E. D. (1977). *Adv. Quant. Chem., 10,* 1.
15. COPPENS, P. (1977). *Angew. Chem., 89,* 33; *Angew. Chem. Int. Ed. Engl., 16,* 32.
16. ABSAR, I. and VAN WAZER, J. R. (1978). *Angew. Chem., 90,* 86; *Angew. Chem. Int. Ed. Engl., 17,* 80.
17. BONHAM, R. A. (1979). *Electron Spectroscopy*, vol. 3, pp. 127–187. London: Academic Press.
18. FUESS, H. (1979). *Modern Physics in Chemistry*, vol. 2, pp. 1–193. London: Academic Press.
19. *Electron and Magnetization Densities in Molecules* (1980) (ed. P. Becker). New York: Plenum Press.
20. *Electron Distributions and the Chemical Bond* (1982) (eds. P. Coppens and M. B. Hall). New York: Plenum Press.
21. (a) REITZ, H. (1975). Thesis, Marburg. (b) HASE, H.-L., REITZ, H. and SCHWEIG, A. (1976). *Chem. Phys. Lett., 39,* 157.
22. HASE, H.-L. and SCHWEIG, A. (1977). *Angew. Chem., 89,* 264; *Angew. Chem. Int. Ed. Engl., 16,* 258.
23. HASE, H.-L., LAUER, G., SCHULTE, K.-W. and SCHWEIG, A. (1978). *Theor. Chim. Acta, 48,* 47.
24. LAUER, G., MEYER, H., SCHULTE, K.-W. and SCHWEIG, A. (1979). *Chem. Phys. Lett., 67,* 503.
25. (a) DANNÖHL, H. (1978). Thesis, Marburg. (b) DANNÖHL, H., MEYER, H. and SCHWEIG, A. (1980). *Chem. Phys. Lett., 69,* 75.
26. HASE, H.-L., SCHULTE, K.-W. and SCHWEIG, A. (1977). *Angew. Chem., 89,* 263; *Angew. Chem. Int. Ed. Engl., 16,* 257.
27. BREITENSTEIN, M., DANNÖHL, H., MEYER, H., SCHWEIG, A. and ZITTLAU, W. (1982). *Electron Distributions and the Chemical Bond* (eds. P. Coppens and M. B. Hall), pp. 255–281. New York: Plenum Press.
28. HIRSHFELD, F. L. (1971). *Acta Cryst., B27,* 769.
29. ROUX, M., BESNAINOU, S. and DAUDEL, R. (1956). *J. Chim. Phys., 53,* 218.
30. BADER, R. F. W., HENNEKER, W. H. and CADE, P. E. (1967). *J. Chem. Phys., 46,* 3341.
31. ROOTHAAN, C. C. J. (1960). *Rev. Mod. Phys., 32,* 179.
32. SMITH, P. R. and RICHARDSON, J. W. (1965). *J. Phys. Chem., 69,* 3346.
33. HEHRE, W. J., LATHAN, W. A., DITCHFIELD, R., NEWTON, M. D. and POPLE, J. A. (1974). *QCPE, 236.*
34. BINKLEY, J. S., WHITEHEAD, R. A., HARIHARAN, P. C., SEEGER, R., POPLE, J. A., HEHRE, W. J. and NEWTON, M. D. (1978). *QCPE, 368.*

35. Present work.
36. BINKLEY, J. S., WHITESIDE, R. A., KRISHNAN, R., SEEGER, R., DEFREES, D. J., SCHLEGEL, H. B., TOPIOL, S., KAHN, L. R. and POPLE, J. A. (1981). *QCPE, 406.*
37. CSIZMADIA, I. G., HARRISON, M. C., MOSKOWITZ, J. W. and SUTCLIFFE, B. T. (1966). *QCPE, 199.*
38. SEEGER, R. *J. Comput. Chem.* (in press).
39. LAUER, G., SCHULTE, K.-W. and SCHWEIG, A. (1978). *J. Am. Chem. Soc., 100,* 4925.
40. COULSON, C. A. and THOMAS, M. W. (1971). *Acta Cryst., B27,* 1354.
41. VON NIESSEN, W., DIERCKSEN, G. H. F. and CEDERBAUM, L. S. (1977). *J. Chem. Phys., 67,* 4124.
42. HERZBERG, G. (1966). *Molecular Spectra and Molecular Structure*, vol. 1. Princeton: Van Nostrand.
43. *Tables of Interatomic Distances and Configuration in Molecules and Ions* (1958) (ed. L. E. Sutton). London: The Chemical Society.
44. SAVARIAULT, J.-M. and LEHMANN, M. S. (1980). *J. Am. Chem. Soc., 102,* 1298.
45. CHRISTIANSEN, P. A. and MCCULLOUGH, JR., E. A. (1977). *J. Chem. Phys., 67,* 1877.
46. MCCULLOUGH, JR., E. A. (1981). *Mol. Phys., 42,* 943.
47. CADE, P. E., SALES, K. D. and WAHL, A. C. (1966). *J. Chem. Phys., 44,* 1973.
48. BANDER, R. F. W. and CHANDRA, A. K. (1968). *Can. J. Chem., 46,* 953.
49. BANYARD, K. E., DIXON, M. and HAYNS, M. R. (1971). *J. Chem. Phys., 54,* 5418.
50. BANYARD, K. E. and HAYNS, M. R. (1971). *J. Phys. Chem., 75,* 416.
51. DUBEN, A. J. and LOWE, J. P. (1971). *J. Chem. Phys., 55,* 4270.
52. DUBEN, A. J. and LOWE, J. P. (1971). *J. Chem. Phys., 55,* 4276.
53. DE WITH, G. and FEIL, D. (1975). *Chem. Phys. Lett., 30,* 279.
54. BECKER, P. (1977). *Physica Scripta, 15,* 119.
55. SMITH, JR., V. H. (1977). *Physica Scripta, 15,* 147.
56. GUNNARSSON, O., HARRIS, J. and JONES, R. O. (1977). *J. Chem. Phys., 67,* 3970.
57. HASE, H.-L., SCHULTE., K.-W. and SCHWEIG, A. (1978). *Z. Naturforsch., 33a,* 245.
58. BICERANO, J., MARYNICK, D. S. and LIPSCOMB, W. N. (1978). *J. Am. Chem. Soc., 100,* 732.
59. PARSONS, C. A. and DYKSTRA, C. E. (1979). *J. Chem. Phys., 71,* 3025.
60. GRAHAM, G. D., MARYNICK, D. S. and LIPSCOMB, W. N. (1980). *J. Am. Chem. Soc., 102,* 4572.
61. WILMSHURST, J. K. and DYKSTRA, C. E. (1980). *J. Am. Chem. Soc., 102,* 4668.
62. MEYER, H. and SCHWEIG, A. (1977). *Z. Naturforsch., 32a,* 1190.
63. FINK, M., GREGORY, D. and MOORE, P. G. (1976). *Phys. Rev. Lett., 37,* 15.
64. BONHAM, R. A. and FINK, M. (1980). *Electron and Magnetization Densities in Molecules and Crystals* (ed. P. Becker), pp. 545–631. New York: Plenum Press.
65. FINK, M. Personal communication.
66. VAN NES, G. J. H. and VAN BOLHUIS, F. (1979). *Acta Cryst., B35,* 2580.
67. Discussions on this point with Prof. A. Vos, Groningen, 1980, are gratefully acknowledged.
68. DANNÖHL, H. and SCHWEIG, A. To be published.
69. PREUSS, H. (1956). *Z. Naturforsch., 11a,* 823.
70. PREUSS, H. (1965). *Z. Naturforsch., 20a,* 21.
71. WHITTEN, J. L. (1966). *J. Chem. Phys., 44,* 359.
72. FRATEV, F., JANOSCHEK, R. and PREUSS, H. (1970). *Int. J. Quant. Chem., 4,* 529.
73. ROTHENBERG, S. and SCHAEFER III, H. F. (1971). *J. Chem. Phys., 54,* 2764.
74. RUSSEGGER, P., LISCHKA, H. and SCHUSTER, P. (1971). *Chem. Phys. Lett., 12,* 392.
75. VLADIMIROFF, T. (1973). *J. Phys. Chem., 77,* 1983.
76. VLADIMIROFF, T. (1974). *Chem. Phys. Lett., 24,* 340.
77. JARVIE, J. O., RAUK, A. and EDMISTON, C. (1974). *Can. J. Chem., 52,* 2778.
78. JARVIE, J. O. and RAUK, A. (1974). *Can. J. Chem., 52,* 2785.
79. BURTON, P. G., CARLSEN, N. R. and MAGNUSSON, E. A. (1976). *Mol. Phys., 32,* 1687.
80. VLADIMIROFF, T. (1976). *J. Chem. Phys., 64,* 433.
81. BURTON, P. G. and CARLSEN, N. R. (1977). *Chem. Phys. Lett., 46,* 48.

82. METZGAR, T. D. and VLADIMIROFF, T. (1977). *Theoret. Chim. Acta., 45,* 235.
83. CARLSEN, N. R. (1977). *Chem. Phys. Lett., 47,* 203.
84. CARLSEN, N. R. and SCHAEFER III, H. F. (1977). *Chem. Phys. Lett., 48,* 390.
85. RYAN, P. B. and TODD, H. D. (1977). *J. Chem. Phys., 67,* 4787.
86. CARLSEN, N. R. (1977). *Chem. Phys. Lett., 51,* 192.
87. NEISIUS, D. and VERHAEGEN, G. (1979). *Chem. Phys. Lett., 66,* 358.
88. WIBERG, K. B. (1980). *J. Am. Chem. Soc., 102, 1229.*
89. NEISIUS, D. and VERHAEGEN, G. (1981). *Chem. Phys. Lett., 78,* 147.
90. DITCHFIELD, R., HEHRE, W. J. and POPLE, J. A. (1971). *J. Chem. Phys., 54,* 724.
91. HEHRE, W. J. and LATHAN, W. A. (1972). *J. Chem. Phys., 56,* 5255.
92. HEHRE, W. J. and POPLE, J. A. (1972). *J. Chem. Phys., 56,* 4233.
93. HEHRE, W. J. (1976). *Accounts Chem. Res., 9,* 399.
94. BONACCORSI, R., PETRONGOLO, C., SCROCCO, E. and TOMASI, J. (1968). *Chem. Phys. Lett., 3,* 473.
95. TYLER, J. K. and SHERIDAN, J. (1963). *Trans. Farad. Soc., 59,* 2661.
96. MCLEAN, A. D. and YOSHIMINE, M. (1968). *IBM J. Res. Develop., 12,* 206, suppl.
97. ALLEN, H. C. and PLYLER, E. K. (1958). *J. Am. Chem. Soc., 80,* 2673.
98. MCLEAN, A. D. and YOSHIMINE, M. (1967). *Tables of Linear Molecule Wave Functions.* San Jose: IBM.
99. BUENKER, R. J. and PEYERIMHOFF, S. D. (1975). *Chem. Phys., 9,* 75.
100. COPPENS, P. and VOS, A. (1971). *Acta Cryst., B27,* 146.
101. VERSCHOOR, G. C. and KEULEN, E. (1971). *Acta Cryst., B27,* 134.
102. DIETRICH, H., SCHERINGER, C., MEYER, H., SCHULTE, K.-W. and SCHWEIG, A. (1979). *Acta Cryst., B35,* 1191.
103. KUTOGLU, A. and HELLNER, E. (1978). *Acta Cryst., B34,* 1617.
104. *See* Ref. 12, p. 119 and Ref. 19, pp. 287 and 355.
105. BECKER, P., COPPENS, P. and ROSS, F. K. (1973). *J. Am. Chem. Soc., 95,* 7604.
106. HANSEN, N. K. and COPPENS, P. (1978). *Acta Cryst., A34,* 909.
107. LITTLE, R. G., PAUTLER, D. and COPPENS, P. (1971). *Acta Cryst., B27,* 1493.
108. COPPENS, P. and HAMILTON, W. C. (1970). *Acta Cryst., A26,* 71.
109. BECKER, P. and COPPENS, P. (1975). *Acta Cryst., A31,* 417.
110. SCHERINGER, C., KUTOGLU, A. and MULLEN, D. (1978). *Acta Cryst., A34,* 481.
111. DRÜCK, V. and GUTH, H. Personal communication.
112. STEVENS, E. D. (1978). *Acta Cryst., B34,* 544.
113. STEVENS, E. D., RYS, J. and COPPENS, P. (1978). *J. Am. Chem. Soc., 100,* 2324.
114. STEVENS, E. D., RYS, J. and COPPENS, P. (1977). *Acta Cryst., A33,* 333.
115. JOHANSEN, H. (1979). *Acta Cryst., A35,* 319.
116. STEVENS, E. D. (1980). *Acta Cryst., B36,* 1876.
117. COPPENS, P. and SABINE, T. M. (1969). *Acta Cryst., B25,* 2442.
118. STEVENS, E. D. and COPPENS, P. (1980). *Acta Cryst., B36,* 1864.
119. GUTH, H., HEGER, G., KLEIN, S., TREUTMANN, W. and SCHERINGER, C. (1980). *Z. Kristallogr., 153,* 237.
120. MULLEN, D. and HELLNER, E. (1978). *Acta Cryst., B34,* 1624.
121. SCHERINGER, C., MULLEN, D., HELLNER, E., HASE, H.-L., SCHULTE, K.-W. and SCHWEIG, A. (1978). *Acta Cryst., B34,* 2241.
122. ELCOMBE, M. M. and TAYLOR, J. C. (1968). *Acta Cryst., A24,* 410.
123. KUTOGLU, A., SCHERINGER, C., MEYER, H. and SCHWEIG, A. (1982). *Acta Cryst., B38,* 2626.
124. KOLLMAN, P. A. and ALLEN, L. C. (1970). *J. Chem. Phys., 52,* 5085.
125. DREYFUS, M. and PULLMAN, A. (1970). *Theoret. Chim. Acta, 19,* 20.
126. DIERCKSEN, H. F. (1971). *Theoret. Chim. Acta, 21,* 335.
127. YAMABE, S. and MOROKUMA, K. (1975). *J. Am. Chem. Soc., 97,* 4458.
128. YAMABE, S., KITAURA, K. and NISHIMOTO, K. (1978). *Theoret. Chim. Acta, 47,* 111.
129. SHERIDAN, R. P. and ALLEN, L. C. (1980). *Chem. Phys. Lett., 69,* 600.
130. OLOVSSON, I. (1980). *Electron and Magnetization Densities in Molecules and Crystals* (ed. P. Becker), pp. 831–894. New York: Plenum Press.

131. DELAPLANE, R. G. and IBERS, J. A. (1969). *Acta Cryst., B25,* 2423.
132. STEVENS, E. D., COPPENS, P., FELD, R. and LEHMANN, M. S. (1979). *Chem. Phys. Lett., 67,* 541.
133. FUESS, H., BATS, J. W., DANNÖHL, H., MEYER, H. and SCHWEIG, A. (1982). *Acta Cryst., B38,* 736.
134. HUZINAGA, S. and SAKAI, Y. (1969). *J. Chem. Phys., 50,* 1371.
135. MÜLLER, U. (1973). *Struct. Bond., 14,* 141.
136. STEVENS, E. D. and HOPE, H. (1977). *Acta Cryst., A33,* 723.
137. BATS, J. W., COPPENS, P. and KVICK, A. (1977). *Acta Cryst., B33,* 1534.
138. DANNÖHL, H. and SCHWEIG, A. Unpublished results.
139. HERMANSSON, K. and LUNELL, S. (1981). *Chem. Phys. Lett., 80,* 64.
140. HERMANSSON, K. and LUNELL, S. (1982). *Acta Cryst., B38,* 2563.
141. LUNELL, S. To be published.